A Comprehensive Overview of Image Enhancement Techniques

Article *in* Archives of Computational Methods in Engineering · April 2021

DOI: 10.1007/s11831-021-09587-6

8 authors, including:

Yunliang Qi
Lanzhou University
36 PUBLICATIONS **502** CITATIONS
SEE PROFILE

Zhen Yang
Lanzhou University
38 PUBLICATIONS **584** CITATIONS
SEE PROFILE

Wenhao Sun
Lanzhou University
16 PUBLICATIONS **311** CITATIONS
SEE PROFILE

Meng Lou
The University of Hong Kong
20 PUBLICATIONS **335** CITATIONS
SEE PROFILE

Archives of Computational Methods in Engineering
https://doi.org/10.1007/s11831-021-09587-6

REVIEW ARTICLE

A Comprehensive Overview of Image Enhancement Techniques

Yunliang Qi[1] · Zhen Yang[1] · Wenhao Sun[2] · Meng Lou[1] · Jing Lian[2] · Wenwei Zhao[1] · Xiangyu Deng[3] · Yide Ma[1]

Received: 23 November 2020 / Accepted: 8 April 2021

Abstract
Image enhancement plays an important role in improving image quality in the field of image processing, which is achieved by highlighting useful information and suppressing redundant information in the image. In this paper, the development of image enhancement algorithms is surveyed. The purpose of our review is to provide relevant researchers with a comprehensive and systematic analysis on image enhancement techniques and give them a valuable reference. Various image enhancement algorithms were mentioned and underlying difficulties, limitations, merits and disadvantages were discussed in applying these techniques in the past two decades with three aspects: supervised algorithm, unsupervised algorithm and quality evaluation, respectively. Further, we summarize some existing problems and analyze the future development trend of existing enhanced algorithms.

1 Introduction

Image enhancement is one of the most important technologies in the field of image processing, and its purpose is to improve the quality of images for specific applications. In general, the basic principle of image enhancement is to modify the information contribution of an image so that it is more suitable for a specific application [1].

Traditional image enhancement methods are mainly based on spatial domain and frequency domain processing. The spatial image enhancement [2] is to directly process the pixels in the image, such as the classic modified histogram methods [3–5], the improved unsharp mask methods [6–8]. The frequency domain image enhancement is to convert the image to the frequency domain in a certain mathematical function such as Fourier transform (FT), discrete cosine transform (DCT) and discrete wavelet transform (DWT), then perform image processing based on the unique properties of the frequency domain, and finally convert it to the original image space. With the rapid development of image enhancement technology, various novel methods have emerged, such as retinex model [9–11], fuzzy theory [12, 13], neural network [14, 15], etc. For example, as shown in Fig. 1, we investigated 162 literatures on image enhancement. The methods involved mainly include histogram equalization, Retinex model, visual cortex neural network and deep learning methods. Each image enhancement method has its own advantages and disadvantages.

The main advantages of spatial domain image enhancement are simple understanding, low complexity and real-time implementation. However, there are also some disadvantages in the spatial domain image enhancement method, such as the lack of sufficient robustness and imperceptibility requirements [16]. It is difficult to propose a method that has a good enhancement for all images. This is mainly caused by the following factors: the non-university of image enhancement algorithm, the choice of evaluation index, the influence of noise and the choice of optimal parameters, etc.

In this paper, we comprehensively provide the progress of image enhancement technology in the past two decades. Based on the latest trends in image processing, we mainly introduce the image enhancement methods separately in three aspects: supervised methods, unsupervised methods and quality evaluation. The block diagram of the whole framework is shown in Fig. 2 in this paper. The rest of paper is organized as follows. Section 2 introduces the image enhancement techniques based on unsupervised algorithms. Section 3 elaborates the supervised algorithms for image enhancement. Section 4 describe in detail the quality

✉ Yide Ma
yidema@gmail.com

[1] School of Information Science and Engineering, Lanzhou University, Lanzhou 730000, Gansu, China

[2] School of Electronic and Information Engineering, Lanzhou Jiaotong University, Lanzhou 730070, Gansu, China

[3] The College of Physics and Electronic Engineering, Northwest Normal University, Lanzhou 730070, China

Published online: 23 April 2021

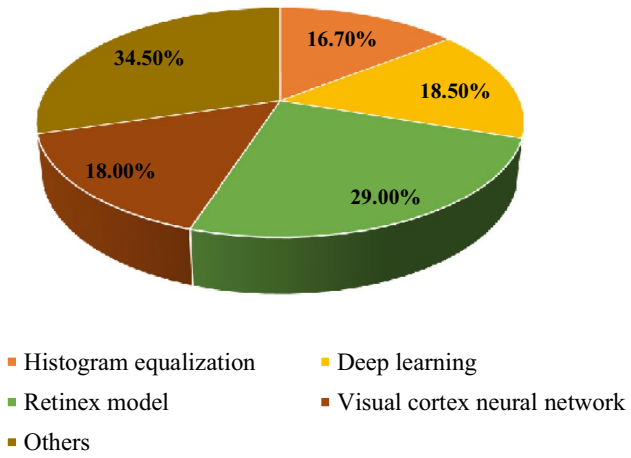

Fig. 1 The statistics of the number of papers with different image enhancement methods

evaluation content of image enhancement. Section 5 makes a conclusion for this paper.

2 Unsupervised Methods

The unsupervised algorithms do not require training samples or training labels, but directly model the data such as K-means [17], hierarchical clustering [18] and EM algorithm [19] etc. In the field of image enhancement, we survey several classic unsupervised algorithms: histogram specification, retinex model and visual cortex neural network. We will introduce in detail as follows:

2.1 Modifying the Histogram of Image

Histogram specification [20] is a method in the field of image processing that uses image histograms to adjust contrast. In this way, the brightness can be better distributed on the histogram. This can be used to enhance the local contrast without affecting the overall contrast. Histogram equalization achieves this function by effectively expanding the commonly used brightness. The histogram of a digital image with a gray level range of $[0, L-1]$ is a discrete function [21]:

$$h(r_k) = n_k \tag{1}$$

where r_k is the k-th grayscale value, and n_k is the number of pixels with r_k in the image. The histogram of an image represents the grayscale distribution of the image.

Generally, we first normalize the histogram and then perform subsequent processing. Assuming that the dimension of the grayscale image is $M \times N$, and M, N represents the total number of pixels in the image, the normalized histogram can be expressed as:

$$p(r_k) = \frac{n_k}{MN}, k = 0, 1, \ldots, L-1 \tag{2}$$

where $p(r_k)$ represents the estimation of the probability of gray level r_k appearing in the image, and the sum of all components of the normalized histogram is equal to 1.

In this section, we mainly elaborate three typical image enhancement methods based on histogram modification: traditional histogram equalization, partial histogram equalization and histogram frequency weighting, respectively.

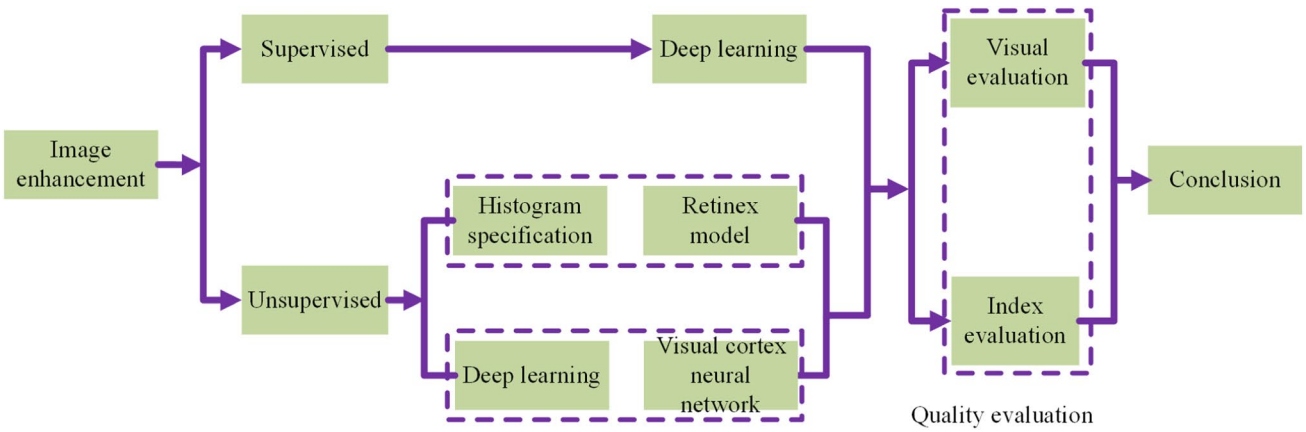

Fig. 2 The whole framework of image enhancement methods

2.1.1 Histogram Equalization

Earlier studies used to render the histograms of all gray levels averagely, but these methods usually overstretch gray levels with larger histogram boxes than others. Histogram equalization(HE) is a common method in image enhancement, which does not require parameter settings of external factors and can effectively enhance image contrast [22]. However, histogram equalization is a method to adjust the image globally, which cannot effectively improve the local contrast, and the effect is very poor in some situations.

Therefore, Karel [23] proposed an Adaptive Histogram Equalization (AHE) method, which calculates the local histogram of image and redistributes the brightness to change the image contrast. That is to say, AHE is more suitable for improving the local contrast of the image and obtaining more image details. An example of image enhancement based on histogram equalization is shown in Fig. 3. Obviously, AHE is better than HE in enhancing the contrast of local details of the image, as shown by the red box in Fig. 3.

2.1.2 Local Histogram Equalization

Traditional histogram equalization(HE) techniques usually cause gray level overlap, local area detail reduction, obvious block effect, blurred background and target contours, etc. In order to preserve the brightness characteristics of the image and better enhance the local details of the image, many scholars have begun to devote themselves to the research of local histogram equalization(LHE) algorithms [4, 24–26]. A typical algorithm flow of local histogram equalization is shown in Fig. 4. Our detailed overview of local histogram equalization methods is as follows:

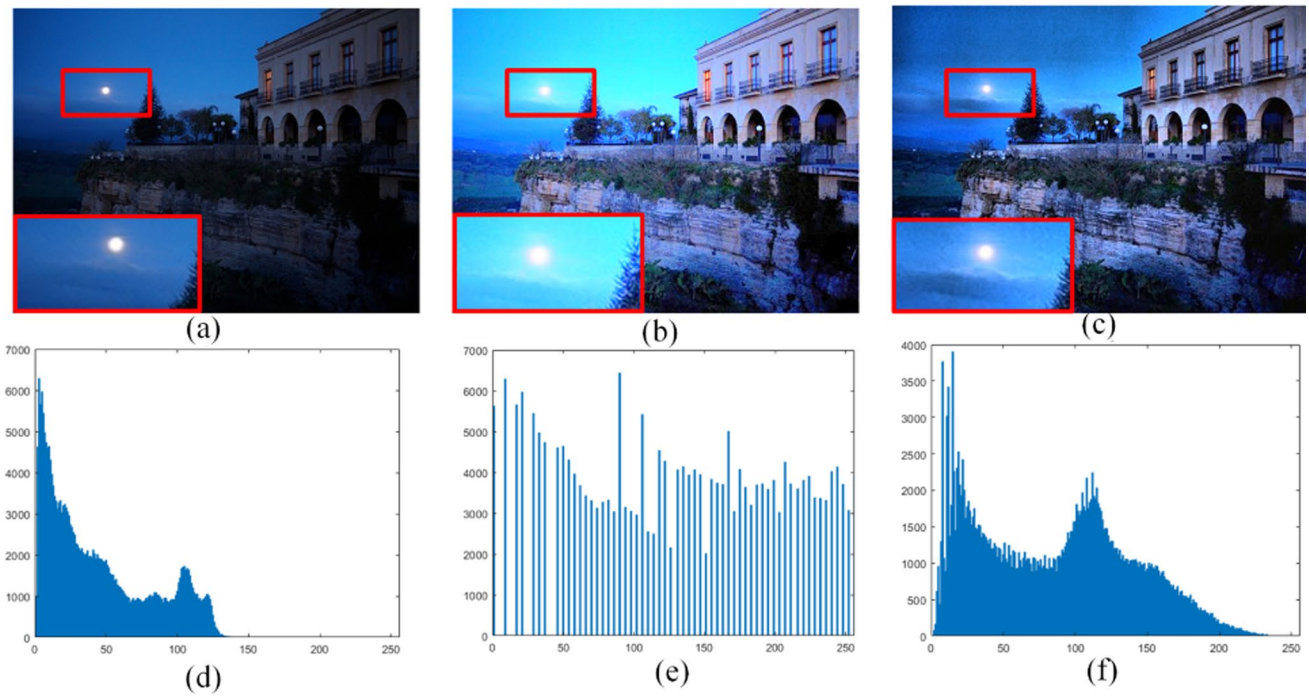

Fig. 3 Image enhancement based on histogram specification. **a** is original image, **b** and **c** are the enhancement results of histogram equalization (HE) and adaptive histogram equalization (AHE), respectively. **d**–**f** are the histograms of (**a**–**c**), respectively

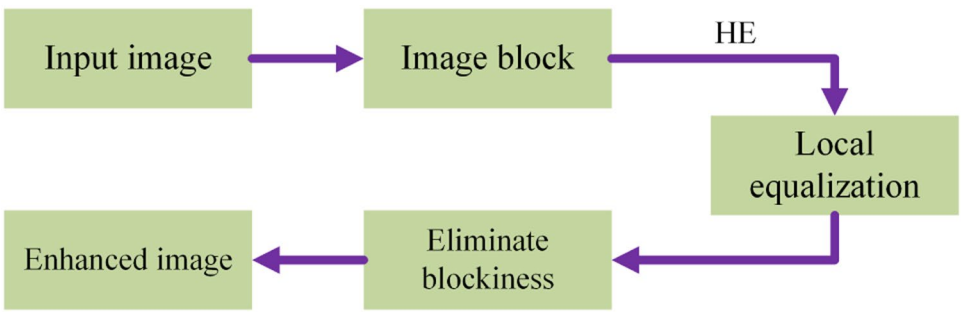

Fig. 4 The algorithm flow of local histogram equalization

In 2001, Kim et al. [27] proposed a partially overlapped sub-block histogram equalization (POSHE), which is the most classic local histogram equalization algorithm. POSHE reduces the blocking effect caused by partial equalization and simplifies the number of equalizations. Lamberti et al. [25] proposed a cascaded multistep binomial filtering histogram equalization (CMBFHE) method based on the POSHE algorithm. They eliminate the blocking effect by constructing a cascaded filter. Specifically, the efficiency of the algorithm is much higher than POSHE algorithm, and the computational complexity is significantly reduced. In addition, a non-overlapped sub-blocks and local histogram projection (NOSHP) is presented by Liu et al. [26]. In their researches, the original image first is divided into lots of non-overlapping sub-blocks, and then histogram projection (HP) is performed respectively. Subsequently, each sub-block is related to its adjacent three sub-blocks with a certain weight, so that the overall image and local details can be enhanced. In recent years, Wang et al. [24] proposed adjacent-blocks-based modification for local histogram equalization (ABMHE), which divides the image into active area, inactive area and general area in advance according to the ratio of the value of the image gradient value, so that local areas in the image can be selected in a targeted manner. The detail enhancement effect of ABMHE algorithm is better than that of POSHE algorithm, but it needs to increase the prior calculation process of image area.

In summary, the local histogram method performs local equalization processing for different spatial location regions, and fully takes into account the local information of the image. Although the local details of the image enhancement method based on local histogram equalization will become richer, the average brightness will usually be greatly affected.

2.1.3 Histogram Frequency Weighting

The histogram frequency weighting technique considers the relationship between histogram equalization and image gray-scale frequency. Specifically, the desired enhancement effect is achieved by adjusting the original frequency of image. In recent years, classic image enhancement methods based on histogram frequency weighting [28–30] have emerged. Specifically, the details are as follows:

WTHE [29] is the most classic histogram frequency weighting method. It modifies the histogram by weighting and thresholding to achieve contrast enhancement. Specifically, WTHE sets two high and low thresholds. For high-frequency gray scales and low-frequency gray scales, the frequency is reduced, and for the gray scales in between, the frequency value is increased by gamma correction, and the total frequency is still 1. The enhanced result obtained by equalizing in this way is much better than the traditional HE algorithm. However, it causes artifacts on some images with slope histogram peaks [31]. In 2011, Yun et al. [32] proposed a contrast enhancement method using a weighted histogram equalization (WHE), which weights the gray value of the HE result and the current gray value setting ratio to get the final result, so that the HE result only occupies a certain proportion. Similar to WHE, Wong et al. [30] performed histogram equalization with maximum intensity coverage. In recent years, researchers have employed the gamma function to modify the existing cumulative distribution function and implement the histogram frequency weighting technique [33, 34].

Finally, in order to show the image enhancement effects of different histogram modification methods, some examples of image enhancement are shown in Fig. 5.

2.1.4 Other Histogram Modification Based Methods

In this paper, considering the limitation of space, we only summarize a few main parts of the method of histogram modification. There are many other image enhancement methods based on histogram modification that have not been listed, such as double histogram equalization, dynamic sub-histogram equalization, transform domain equalization and histogram clipping. Here we briefly summarize.

Double histogram equalization is to decompose the original histogram into two histograms, and then equalize the two histograms separately. Typical methods are brightness preserving bi-histogram equalization [35] (BBHE), dualistic sub-image histogram equalization [4](DSIHE), minimum mean brightness error bi-histogram equalization [36] (MMBEBHE). In recently years, the double histogram equalization technology combines the ideas of image analysis, such as the local equalization of the background area, target area, texture area, and smooth area [37, 38]. The dynamic histogram equalization takes into account the curve distribution of the histogram, and then selects the appropriate area for equalization. Typical methods are DHE [39] and BPDHE [40]. In addition, there are also transform domain histogram equalization [41–43] and histogram clipping [44–46], etc.

2.2 Retinex-Based Enhancement

The Retinex theory was proposed by Land et al. [47] in 1968, which is based on the principle of retinal imaging to simulate the human visual system (HVS). In this theory, it is assumed that image lightness depends on illumination and reflectance. The Retinex algorithm [48] was proposed based on the fact that when the human visual system judges the true color of an image, it is hardly disturbed by light. In this section, we elaborate the contents of the Retinex model as follows:

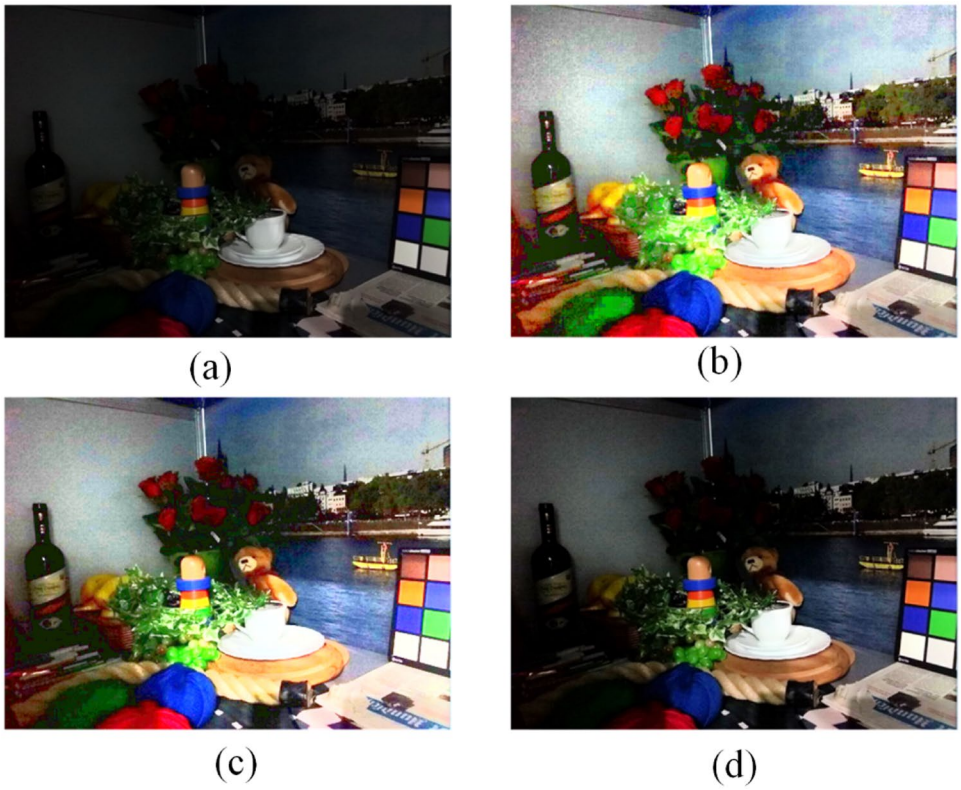

Fig. 5 Image enhancement based on histogram modification.**a** is the original image. **b**, **c** and **d** are the enhanced results of POSHE [27], WTHE [29] and AGCWD [33], respectively

2.2.1 Basic Retinex Algorithm

According to Land et al. [47–49], color vision is not determined by the intensity of visible light irradiated to the human eye, but the inherent reflectivity of the surface of the object. The human eye can filter out the influence of light in some way and directly obtain the reflectivity of the surface of the object to determine colour. Therefore, the formation of a low-light image can be described as follows:

$$L(x, y) = R(x, y) \cdot B(x, y) \tag{3}$$

where $L(x, y)$ is the original image, $R(x, y)$ is the reflection image, $B(x, y)$ is the illuminance image and (x, y) is the pixel coordinates.

Generally, Retinex performs image processing based on two methods: one is to divide the color image into three RGB channels and the Retinex algorithm is applied to each channel to solve the color shift problem. The other is to convert the image to a brightness channel in the color model (such as HSV color model, CIELuv color model) and its brightness channel is processed separately to solve the problem of uneven illumination.

2.2.2 Path-Based Retinex Algorithm

The path-based Retinex algorithm [50] is the most basic Retinex model. Its basic idea is to use the local brightest point in the path-White Patch [51] (WP) to calculate the relative brightness of adjacent pixels in the path to obtain the reflection component. Given a normalized input image $L(x)$, a path can be selected from a certain point y to the target point x in the image. Assume that the brightness values of two adjacent pixels on the path are $S(x_k)$ and $S(x_{k+1})$ respectively. Then the relative brightness value at x can be obtained along this path:

$$R\hat{}(x) = \prod_{m=1}^{n-1} \delta_\varepsilon \left(\frac{S_{m+1}}{S_m} \right) \tag{4}$$

where n is the number of pixels on the path and δ_ε is threshold function. In order to enhance the robustness of the algorithm, the relative pixel brightness of x at multiple paths can be expressed as:

$$R(x) = \frac{1}{N} \sum_{k=1}^{N} R_k\hat{}(x) = \frac{1}{N} \sum_{k=1}^{N} \prod_{m_k=1}^{n_k-1} \delta_\varepsilon \left(\frac{S_{m_k+1}}{S_{m_k}} \right) \tag{5}$$

where N is the number of paths. In 2005, Provenzi et al. [52] proved that the threshold mechanism has very little contribution to the model algorithm, so (5) can be simplified as:

$$R(x) = \frac{1}{N} \sum_{k=1}^{N} \prod_{m_k=1}^{n_k-1} \left(\frac{S_{m_k+1}}{S_{m_k}} \right) \tag{6}$$

For the path-based Retinex algorithm, the researchers have focused on the selection of the pixel path, and lots of related work has gradually emerged. Marini et al. [53] used a random midpoint displacement method so that the path chosen is close to Brownian motion. Cooper et al. [54] used a double helix method to select the path. Their method has achieved good results in reducing noise. However, since the sampling method of the path is one-dimensional and depends on the direction information, rather than the neighborhood information, the processed image is prone to appear halo, artifacts, etc [55–57]. In order to solver this problems, therefore, Provenzi et al. [58] proposed a two-dimensional Random Spay Retinex (RSR). In the work of Provenzi et al. [58], the path method is designed to scatter points in a two-dimensional circle, and the density of the circular scatter points at the center x distance r is controlled by the density function. The algorithm is described as follows:

$$R(x) = \frac{1}{N}\sum_{k=1}^{N}\frac{L(x)}{\max\left\{L(i), i \in P_k(x)\right\}} \tag{7}$$

where $P_k(x)$ indicates the area of the k-th spot, $L(x)$ is the input image. Based on the work of Provenzi et al., the researchers have begun to improve the algorithm, such as the LRSR [59] (Light random sprays Retinex) model and SLRMSR [60] (Smart light random memory sprays Retinex) model proposed by Banic and Loncaric. In addition, Bertalmio et al. [61] proposed a kernel-based Retinex model, which replace the two-dimensional spay process with a more efficient kernel.

Path-based Retinex algorithm can effectively improve the image contrast. However, due to the uncertainty of its initial position, end position and path selection, it is easy to introduce undesirable noise and affect the accuracy of illumination estimation. Besides, the computational complexity is high, so that it is inconvenient to apply in practice, and it is difficult to obtain high-quality pictures with high color fidelity and good visual effects.

2.2.3 Retinex Algorithm Based on Center/Surround

The Retinex center/surround model was first proposed by Land [62], and its core idea is to estimate the illuminance component with a Gaussian kernel function. According to Land [62], it is considered that the Retinex result of a certain point of the image should be the ratio of the luminous intensity of that point to the average luminous intensity of the adjacent positions. In addition, the Mach zone phenomenon is explained through experiments and the rationality of the method is established. Typical Retinex center/surround models include single-scale Retinex (SSR) [9] algorithm, multi-scale Retinex (MSR) [63] algorithm and multi-scale Retinex with color restoration factor (MSRCR) [11] algorithm.

According to [9], SSR model can be described as:

$$R_i(x,y) = \log I_i(x,y) - \log\left[F(x,y) * I_i(x,y)\right] \tag{8}$$

where I_i is the image distributed in the i-th color band, $R_i(x,y)$ is the enhancement result, * means convolution operation, $F(x, y)$ represents the convolution kernel function and the formula is as follows:

$$F(x,y) = k \cdot \exp\left(-\frac{x^2+y^2}{2\sigma^2}\right) \tag{9}$$

where k needs to satisfy $\iint F(x,y)\mathrm{d}x\mathrm{d}y = 1$. σ represents kernel parameter, which can determine the enhancement effect of image. Specially, the larger (smaller) σ is, the richer (weaker) the image detail information will be, and the lower (higher) the color fidelity will be.

The enhancement effect of the SSR model is closely related to the size of the Gaussian kernel. For a grayscale image, a small Gaussian kernel can increase the brightness of the dark parts of the image, but it may cause excessive compensation and make the dynamic range of the image too small, ie., "halo" phenomenon. A large Gaussian kernel can increase the dynamic range of the image, but may make the model lose its local characteristics, and the shadow of the image cannot be compensated. Therefore, Rahman et al. [63] proposed the MSR algorithm. The basic idea of the algorithm is to sum multiple Gaussian kernel scale parameters by weight and its expression is as follows:

$$\begin{aligned}\mathfrak{R}_m(x,y) = &\sum_{n=1}^{N}\omega_m \\ &\left[\log I_m(x,y) - \log\left(F_m(x,y) * I_m(x,y)\right)\right]\end{aligned} \tag{10}$$

where $F_m(x,y)$ is the filter kernel function, and the scale and the total number of scales are δ_m and N respectively. ω_m is the weighting factor corresponding to the m-th parameter, which satisfies $\sum \omega_m = 1$.

In order to reduce the color cast and restore the true color of the image, a multi-scale Retinex algorithm with color restoration factor(MSRCR) [10, 11, 64] was proposed. The model algorithm is expressed as follows:

$$\aleph = c_i(x,y) \cdot \mathfrak{R}_m(x,y) \tag{11}$$

where $\aleph$ is the enhanced result of image, $c_i(x,y)$ is the color restoration factor and its expression is as follows:

$$c_i(x,y) = \mu \cdot \log\left(\eta \cdot \frac{I_i(x,y)}{\sum_i I_i(x,y)}\right) \tag{12}$$

where μ and η are the gain factor and offset that affect the color recovery of the image, and both are constant, I_i is the image distributed in the i-th color band.

Wang and Luo [65] improved Jobson's [9] method and proposed a multi-layer image enhancement model. Although the Retinex algorithms based on center/surround have a good effect in terms of color fidelity, the time complexity is high, the halo phenomenon is obvious and image distortion is inevitable. Some examples of Retinex algorithm enhancement based on center/surround are shown in Fig. 6. From Fig. 6, we can see that the center/surround-based Retinex algorithm can effectively enhance the contrast of the image. However, the parameter settings in the algorithm have limitations, resulting in uncertainty in the contrast, chroma, and clarity of the enhanced image, so the enhancement effect is not ideal. Specially, the SSR algorithm can slightly improve the color of the sky, but the overall contrast is reduced, and the halo phenomenon is more serious. in Fig. 6f, the MSRCR algorithm has a color factor, and the color is obviously better than that of the MSR algorithm in Fig. 6e. With the in-depth research of the Retinex algorithm by scholars, especially for the two major defects of color distortion and halo in the traditional Retinex algorithm, a large number of improved algorithms have been proposed.

2.2.4 Partial Differential Equations(PDE) model

As a matter of fact, the basic Retinex algorithm is a calculation theory of color vision, and its details are not described mathematically [66]. In 1974, Horn et al. [67] simplified the Retinex model for the first time based on partial differential equations (PDE). For (3), they separated the illumination component $B(x, y)$ and the reflection component $R(x, y)$ from $L(x, y)$ and constructed the partial differential equations. Take the logarithm of both sides of (3) to get:

$$\mathcal{L}(x, y) = \mathcal{R}(x, y) + \mathcal{B}(x, y) \tag{13}$$

where $\mathcal{L}(x, y) = \log L(x, y)$, $\mathcal{R}(x, y) = \log R(x, y)$, $\mathcal{B}(x, y) = \log B(x, y)$. Then, from (13) we can get:

$$\Delta\mathcal{L}(x, y) = \Delta\mathcal{R}(x, y) + \Delta\mathcal{B}(x, y) \tag{14}$$

where Δ is Laplacian. In addition, the following algorithm can be defined as:

$$\delta_\varepsilon(\Delta\mathcal{L}(x, y)) = \begin{cases} \Delta\mathcal{L}(x, y), & |\Delta\mathcal{L}(x, y)| > \varepsilon \\ 0, & else \end{cases} \tag{15}$$

According to Horn et al. [67], under the premise of uniform illumination, the illumination map $B(x, y)$ is smooth everywhere, and its partial derivative is a very small value. Thus, we get $\delta_\varepsilon(\Delta\mathcal{L}(x, y)) \approx \Delta\mathcal{R}(x, y)$. Finally, its Poisson equation is as follows:

$$\Delta\hat{\mathcal{R}}(x, y) = \delta_\varepsilon(\Delta\mathcal{L}(x, y)) \tag{16}$$

Horn first proposed to use an iterative strategy to solve it, but this is not the optimal method [56]. Blake et al. [68–70] improved Horn's method by using a gradient method. Morel et al. [71, 72] derived a similar Poisson equation based on the path-based Retinex model. In addition, they proved that the Retinex model can be characterized as a discrete Poisson

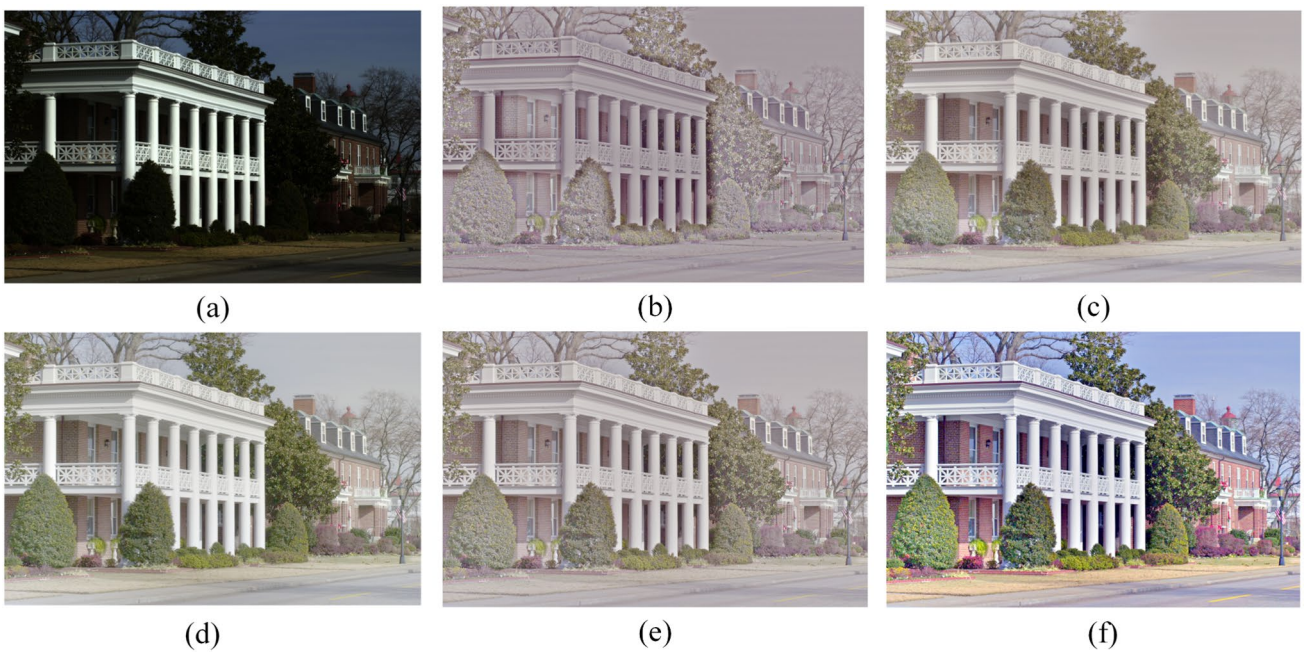

Fig. 6 Some examples of Retinex algorithm enhancement based on center/surround.**a** is the original image. **b–f** are the enhanced results of SSR with $\delta = 15$ [9], SSR with $\delta = 80$, SSR with $\delta = 250$, MSR($\delta_1 = 15, \delta_2 = 80, \delta_3 = 250$) [63] and MSRCR [11], respectively

equation with Neumann boundary conditions and expressed as follows:

$$\begin{cases} -\Delta_d \mathcal{R}(x,y) = \sum\limits_{x_0 \in N_4(x,y)} \delta_\varepsilon(\mathcal{L}(x,y) - \mathcal{L}(x_0,y_0)), x \in \Omega \\ \frac{\partial_d \mathcal{R}(x,y)}{\partial n} = 0,\ x \in \partial\Omega \end{cases} \tag{17}$$

where Δ_d and ∂_d represent the discrete Laplace operator and discrete partial differential symbols respectively. It can be seen that (17) and (16) are equivalent without considering the threshold function δ_ε. Ma et al. [73] analyzed Poisson equation (17) in detail and concluded that the solution can be regarded as an optimization problem of L2 norm, that is, L2-Retinex. Then,

$$\hat{\mathcal{R}} = \arg\min_R \left\{ \left\| \Delta\mathcal{R} - \delta_\varepsilon(\Delta\mathcal{L}(x,y) \right\|_2^2 \right\} \tag{18}$$

Similarly, they also proposed a L1-Retinex model [74], which is expressed as follows:

$$\hat{\mathcal{R}} = \arg\min_R \left\{ \left\| \Delta\mathcal{R} - \delta_\varepsilon(\Delta\mathcal{L}(x,y) \right\|_1 \right\} \tag{19}$$

In summary, the PDE model constructs partial differential equations based on some basic assumptions of Retinex theory, and its description is more accurate than the path-model. In addition, the PDE model has fewer parameters and the results obtained are more stable.

2.2.5 Retinex Models Based on Variational Methods

In image enhancement, in order to effectively eliminate the halo, scholars proposed the Retinex algorithm based on the variational framework, also known as the Retinex-like model. Classical variational models usually include two types: the HVS-based variational model and the Horn physical prior variational model.

A. The HVS-based Variational Model

Palmaamestoy et al. [75] first proposed the Retinex-like variational model based on HVS. In their method, the subject model is described as:

$$E_\omega(I) = D(I) + C_\omega(I) \tag{20}$$

where $E_\omega(I)$ is defined as the color correction energy functionl, $D(I)$ is the dispersion term and $C_\omega(I)$ is the contrast term. The global item $D(I)$ is used to control the final generated image and satisfies the GW (Gray world) assumption [76]. Minimizing $C_\omega(I)$ can enhance the local contrast of the image, which has certain characteristics of the Retinex model. In particular, Palmaamestoy choose the dispersion energy as the global term $D(I)$. The final optimized result is close to the original image I_0 and satisfies the GW assumption, that is, the final result is close to 1/2. The entropic dispersion term $D(I)$ is defined as follows:

$$\begin{aligned} D^\varepsilon_{\alpha,\beta}(I) := \alpha \sum_{x\in\Upsilon} \left(\frac{1}{2}\log\frac{1}{2I(x)} - \left(\frac{1}{2} - I(x)\right) \right) \\ + \beta \sum_{x\in\Upsilon} \left(I_0(x)\log\frac{I_0(x)}{I(x)} - \left(I_0(x) - I(x)\right) \right) \end{aligned} \tag{21}$$

where $\alpha, \beta > 0$. In addition, the contrast term is described as follows:

$$C^f_\omega(I) := \frac{1}{4} \sum_{x\in\Upsilon} \sum_{y\in\Upsilon} \omega(x,y) f\left(\frac{\min(I(x), I(y))}{\max(I(x), I(y))} \right) \tag{22}$$

where $\omega(x,y)$ is the distance function, and its value decreases monotonously with the increase of the distance between pixels. $\omega(x,y)$ can be used to achieve "local" characteristics and f represents the gamma correction function. The Retinex-like model has the disadvantage of a large calculation. Therefore, Provenzi et al. [77] combined with wavelet based on Palmaamestoy et al.'s variational model to reduce the amount of calculation.

B. Horn's Physical Prior based Retinex

Kimmel et al. [78] believed that the spatial variation of the illumination component is smooth. According to the priori assumption, based on Horn's work [67], they proposed a variational form of Retinex and the penalty functional is as follows:

$$\begin{aligned} Minimize: F[\mathcal{B}] = \iint_\Omega \\ \left(|\nabla\mathcal{B}|^2 + \alpha(\mathcal{B}-\mathcal{L})^2 + \beta|\nabla(\mathcal{B}-\mathcal{L})|^2 \right) dxdy \\ Subjectto: \mathcal{B} \geq \mathcal{L} and \langle \nabla\mathcal{B}, \vec{n} \rangle = 0 on \partial\Omega, \end{aligned} \tag{23}$$

where Ω is the support of the image, $\partial\Omega$ is the partial differential of the image, etc., the boundary, and $\vec{n}$ is the normal to the boundary. α, β are non-negative real parameters and are used to control the importance of the corresponding items. The first penalty term $|\nabla\mathcal{B}|^2$ ensures that the final illumination component is smooth, and the second term $(\mathcal{B}-\mathcal{L})^2$ is a fidelity term, which ensure that the difference between $\mathcal{B}$ and $\mathcal{L}$ is not too large. The third item $|\nabla(\mathcal{B}-\mathcal{L})|^2$ is equivalent to $|\nabla(\mathcal{R})|^2$, and its function is to obtain the spatial distribution of the reflected components as smooth as possible, so as to obtain a better visual effect. Since then, some novel models have been constructed based on the Kimmel et al.'s model by modifying or adding some constraints [79–81], which reflects the flexibility of the variational method. Ma and Osher [81] introduced

a total variation (TV) noise suppression model [82] to estimate the image illumination component. Their model is described as follows:

$$Minimize : F[\mathcal{B}] = \iint_{\Omega} \frac{1}{2}\left(\|\nabla\mathcal{B}\|_2^2 + t\|\nabla\mathcal{R}\|_2\right)dxdy \tag{24}$$

where $\|\nabla\mathcal{B}\|_2$ is the TV term, which is used to obtain a piecewise smooth reflection map, t is the weight coefficient. Ng and Wang [80] added fidelity items based on Ma and Osher's works and obtain:

$$Minimize : F[\mathcal{B}] = \iint_{\Omega} \left(\frac{\alpha}{2}\|\nabla\mathcal{B}\|_2^2 + \|\nabla\mathcal{R}\|_2 + \frac{\beta}{2}\|\mathcal{B}-\mathcal{R}-\mathcal{L}\|^2\right)dxdy \tag{25}$$

where $\|\mathcal{B}-\mathcal{R}-\mathcal{L}\|^2$ is the fidelity term, α and β are the weight coefficients. The variational model based on physical prior conditions is relatively flexible, and different constraints can be easily added to obtain better results.

C. Other Retinex-like Models

In recent years, a large number of Retinex-like models have been also emerging. Fu et al. [83] proposed a probabilistic model for image enhancement (PIE). A Maximum a Posteriori (MAP) was used in Fu et al.'s method to estimate reflectance and illumination in the linear domain. Finally, to effectively decompose the illumination and reflectivity, the MAP problem is transformed into an energy minimization problem. The Alternating Direction Multiplier Method (ADMM) [84] is used to simultaneously estimate the illumination and reflectance components. In particular, PIE is a processing algorithm based on linear space. Compared with the logarithmic domain processing algorithm, PIE has the advantages of preserving details well and avoiding over-smooth reflection components. In 2016, related work of [85] proposed a weighted variational model for simultaneous reflectance and illumination estimation (SRIE) with more details. In their method, noise can be suppressed to a certain extent. However, the unconstrained assumption of isotropy may destroy the illumination component.

Guo et al. [86] proposed a low-light image enhancement (LIME) method via illumination map estimation. Specially, a structure prior is imposed to refine the illumination map. On the basis of Max-RGB [47], they considered the defect that it can only boost global illumination, and introduced the following initial estimation:

$$\hat{B}(x,y) \leftarrow \max_{c\in\{R,G,B\}} L^c(x,y) \tag{26}$$

According to Guo et al.'s researches, $\hat{B}(x,y)$ in (26) guarantees that the recovery will not reach saturation. Although LIME has a good effect on low-light image enhancement, it can't solve the problem of over-enhancement of illumination, because that it adds to the noise amplification. In recent years, related works in large numbers have taken noise as an important factor of Retinex-like, and proposed some low-light image enhancement models. Li et al. [87] proposed a Retinex model with a definite injected noise term, and for the first time tried to estimate the noise map based on the model. Ren et al. [88] proposed a Low-Rank Regularized Retinex Model (LR3M). They injected low-rank priors into the Retinex decomposition process for the first time and suppressed noise in the reflection map. Unlike the method of Li et al. [87], LR3M is full aware of noise and performs adaptive processing throughout the enhancement process. Recently, Xu et al. [89] proposed a structure and texture aware Retinex (STAR) model. In their method, STAR model is solved based on an alternating optimization algorithm. In addition, each sub-problem is transformed into a vectorized least squares regression, with closed-form solutions. Tang et al. [90] proposed a new prior constraint, ie., local flatness. Different from the previous works, they selectively add local flatness to the illumination by calculating the deviation between the estimated illumination map and the reference map.

Finally, some examples of Retinex algorithm enhancement based on variational methods for low-light image enhancement are shown in Fig. 7. Intuitively, the overall contrast enhancement of PIE [83] and SRIE [85] is not satisfactory. LIME [86] does not preserve the details of image well.

2.3 Visual Cortex Neural Network Based Enhancement

The visual cortex neural networks were proposed to simulate the mammalian visual cortex system. In recent years, a large number of visual cortex neural network models have been developed. Among them, Eckhorn model [91, 92], Parodi model [93] and Rybak model [94] are the most representative visual cortex models. Further, the pulse coupled neural network (PCNN) evolved from the Eckhorn model has been extensively and deeply studied by researchers. In this section, we mainly focus on two classic visual cortex neural networks: PCNN and Rybak model, to review image enhancement methods.

2.3.1 Basic PCNN Model and Image Enhancement

PCNN, the third generation neural network, was inspired by the visual cortex of cats and evolved from the Eckhorn model. As a single layer neural network that does not require any training [95], PCNN has been widely applied in image processing [96], based on its biological background mechanism. The basic PCNN is elaborated in Ranganath et al.'s work [96]. Furthermore, Lindblad et al [97] gave the discrete expression of the basic PCNN model as follows:

$$F_{ij}[n] = e^{-\alpha_f} F_{ij}[n\text{ - }1] + V_F \sum_{kl} M_{ilkl} Y_{kl}[n-1] + S_{ij} \tag{27}$$

$$L_{ij}[n] = e^{-\alpha_l} L_{ij}[n\text{ - }1] + V_L \sum_{kl} W_{ilkl} Y_{kl}[n-1] \tag{28}$$

$$U_{ij}[n] = F_{ij}[n]\left(1 + \beta L_{ij}[n]\right) \tag{29}$$

$$Y_{ij}[n] = \begin{cases} 1, & if \quad U_{ij}[n] > E_{ij}[n] \\ 0, & else \end{cases} \tag{30}$$

$$E_{ij}[n] = e^{-\alpha_e} E_{ij}[n\text{ - }1] + \mathrm{V}_E \mathrm{Y}_{ij}[n] \tag{31}$$

Obviously, a basic PCNN neuron $N(i, j)$ embedded in a 2-D array is mainly composed of two important parts: feedback input F_{ij} and linking input L_{ij}. Neighboring neurons communicate with each other through the two synaptic weights M_{ilkl} and W_{ilkl} respectively. In addition, the previous state altered by the attenuation factors $e^{-\alpha_f}$ and $e^{-\alpha_l}$ are also contained in the current feedback input F_{ij} and linking input L_{ij}. The input S_{ij} is only included in the feedback input F_{ij}. The feedback input F_{ij} and linking input L_{ij} are combined with a link factor β to obtain an internal activity U_{ij}. Then, the output Y_{ij} is obtained through the comparison of internal activity U_{ij} and dynamic threshold E_{ij}. Finally, the activation state of the neuron is determined, that is, the output Y_{ij} is 1 (activated) or 0 (not activated). The threshold E_{ij} is dynamic, because when the neuron is activated, the threshold would increase by the amplification item V_E. Otherwise, the dynamic threshold would decay by the factor $e^{-\alpha_e}$ until the neuron activates again. The parameters n is the discrete iteration time of the neuron, V_F and V_L are the amplitudes of feedback input F_{ij} and linking input L_{ij} respectively, α_f, α_l and α_e are the exponential decay coefficients of feedback input, linking input and dynamic threshold, respectively.

In 2003, Zhang and Lu [98] studied the relationship between PCNN and human visual characteristics and applied it to image enhancement. Early literature [99] shows that the brightness perceived by the human visual system is different from the brightness of the light source, and it has a logarithmic relationship with the illuminance obtained by the human eye. In addition, the brightness perceived by human is not a simple function of light intensity, such as the Mach band effect [99, 100]. The logarithmic transformation characteristic of the image is shown in Fig. 8. The horizontal axis x is the pixel intensity of the image, where *Dark* is the darkest gray scale value of the image and *Bri* is the brightest gray scale value. In Zhang and Lu's work, the enhanced image is defined as the excited grayscale image perceived by PCNN as follows:

$$EnI_{ij} = In(Bri) - (n-1)\alpha_e \tag{32}$$

where EnI_{ij} is the perceptual excitation value of the (i, j)-th pixel in the enhanced image, $ln(*)$ is logarithmic transformation and n is the activated times (n=1, 2, 3, …) of PCNN. For the basic PCNN model, the parameters are set as follows:

$$M_{ijkl} = W_{ijkl} = \frac{1}{(i-k)^2 + (j-l)^2} \tag{33}$$

That is, the synapse weight between neurons is defined as the inverse of the square of the Euclidean distance [96, 101, 102]. The threshold exponential decay coefficient α_e is a small value and is set to 0.001. In addition, (27) is usually simplified to $F_{ij}[n] = S_{ij}$. $V_L = 1$.

Based on this theory, many scholars have proposed image enhancement algorithms for specific applications based on PCNN [103–106]. In summary, the image enhancement algorithm based on PCNN can be described as follows:

Algorithm 1: Enhancement by PCNN model.

Input : The gray image S_{ij}
Output: The enhancement result Y for each image.

Initial the parameters of PCNN.
Calculate W_{ijkl} and M_{ijkl} according to (33), calculate F_{ij} and L_{ij} according to (27) and (28), respectively.
$n = 0$
while $n < N$ **do**
  $n = n + 1$
  update E_{ij} by (31).
  reapt.
  update U_{ij}, Y_{ij} according to (29), (30).
  calculate EnI_{ij}.
  $Y_0 = Y_{ij} \cdot EnI_{ij}$
  if $any\,(Y\,(:)) == 0$
    break;
  end
end while
Normalize linearly Y_0 to obtain Y.

Based on the capture characteristics and synchronous oscillation characteristics of PCNN, Li et al. [107–109] combined genetic algorithm and Otsu theory, etc., proposing many image enhancement algorithms with PCNN noise reduction characteristics. In addition, Qi et al. [110] proposed a feedback pulse-coupled neural network (FPCNN) and applied it to image enhancement. In their work, the input image is first denoised by PCNN, and then segmented by PCNN, and the continuous output of multiple binary images is logically "OR" and "exclusive or (EOR)" operations to obtain image texture, edge and other information. Finally, these information is combined with the original image to form an enhanced image. In 2019, Nie et al. [111] proposed to employ the classical visual receptive field (CVRF), improving pulse coupled neural network (PCNN) and conducted a contrast enhancement of MRI images.

2.3.2 Time Matrix of PCNN

In addition to the human eye's method of perceiving brightness, namely (32), the time matrix is also one of the most important tools for image enhancement. The time matrix is defined to record the first firing time of each PCNN neuron [112]. In 2009, Zhan et al. [113] found that the sensitivity of the time matrix is inversely related to the intensity of the image pixels.

A neuron fires when its membrane potential is greater than the threshold. Then, the threshold would decay exponentially from the first predetermined $E_{ij}(0)$ by (31). That is, the neuron (i, j) is firing at the time T_{ij} when

$$U_{ij}\left(T_{ij}\right) > E_{ij}\left(T_{ij}\right) = e^{T_{ij}} E_{ij}(0) \tag{34}$$

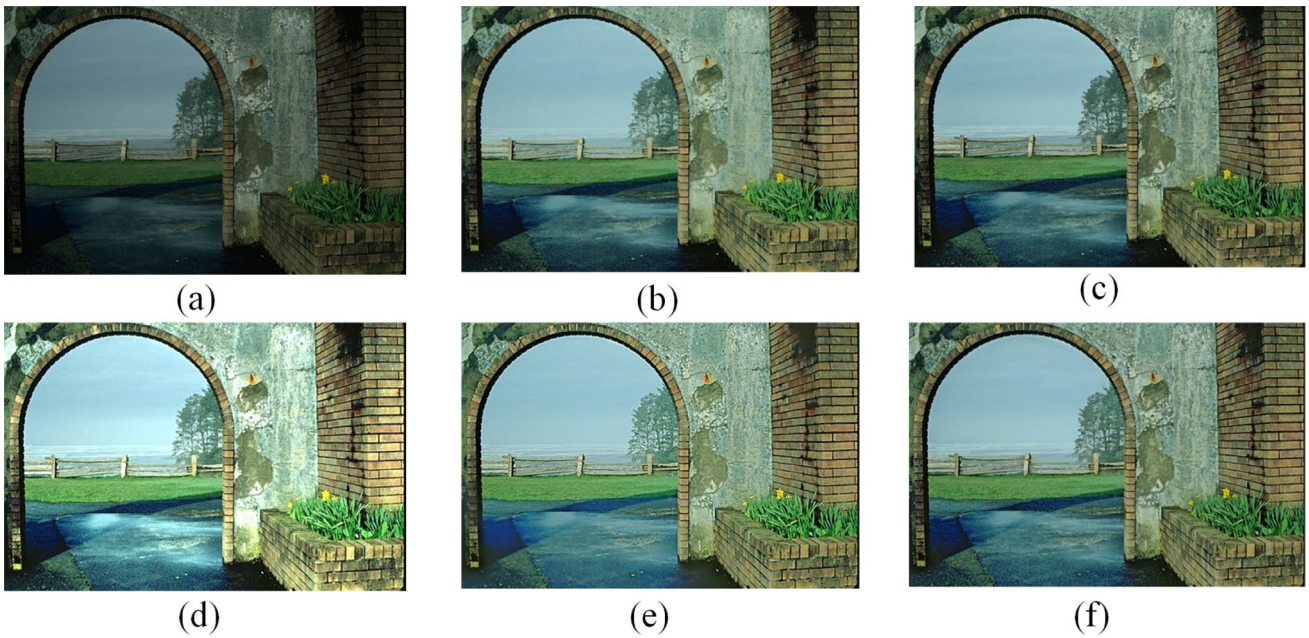

Fig. 7 Some examples of Retinex algorithm enhancement based on variational methods.**a** is the original image. **b**–**f** are the enhanced results of PIE [83], SRIE [85], LIME [86], Li et al. [87] and Tang et al. [90] respectively

Therefore, the first firing time T_{ij} can be obtained from (34),

$$T_{ij} = \mathrm{In}\frac{U_{ij}(T_{ij})}{E_{ij}(0)} \tag{35}$$

From (35) we get the analytical solution of the time matrix T_{ij}, but T_{ij} still cannot be obtained because (35) is an implicit function. In implementation, the time matrix can be obtained according to the following formula [114]:

$$T_{ij}(n) = T_{ij}(n-1) + nY_{ij}(n) \tag{36}$$

The premise that the time matrix can be obtained is that the threshold amplitude factor V_E must be large enough to ensure that the neuron fires only once. Therefore, the time matrix of PCNN can be obtained by the following Algorithm 2.

Algorithm 2: The time matrix of PCNN.

Input : The gray image S_{ij}
Output: The time matrix T_{ij} for each image.
1: Initial the parameters of PCNN.
Calculate W_{ijkl} and M_{ijkl} according to (33), calculate F_{ij} and L_{ij} according to (27) and (28), respectively.
2: $firednum = 0$, $n = 0$.
3: **while** $n < N$ **do**
4: $n = n + 1$
5: update E_{ij} by (31).
6: reapt.
7: update U_{ij}, Y_{ij} according to (29), (30).
8: $firednum = firednum + sum(Y)$
9: $T = T + nY$
10: **end while**

2.3.3 Spiking Cortical Model (SCM)

The spiking cortical model (SCM) is a variant model of PCNN, which was proposed by Zhan et al. [113] in 2009. It consists of a leakage integrator, linking input and feedback input as follows

$$U_{ij}[n] = fU_{ij}[n-1] + S_{ij}\sum_{kl} W_{ijkl}Y_{kl}[n-1] + S_{ij} \tag{37}$$

The dynamic threshold item directly inherits the settings of the basic PCNN model and is expressed as:

$$E_{ij}[n] = gE_{ij}[n-1] + hY_{ij}[n-1] \tag{38}$$

Furthermore, the sigmoid activation function is employed as the ignition condition of SCM neurons and is described as follows,

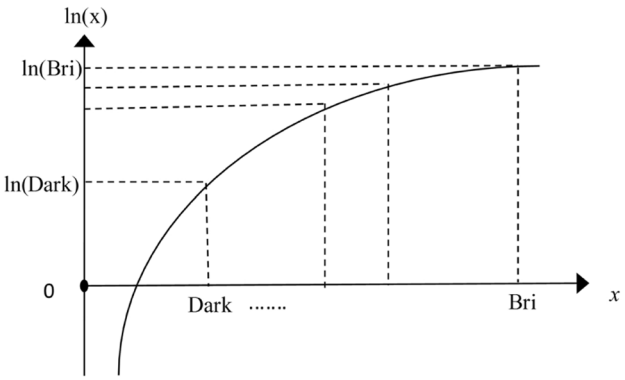

Fig. 8 Logarithmic transformation properties of image

$$Y_{ij}[n] = \begin{cases} 1, & 1/(1+\exp(-\gamma(U_{ij}[n] - E_{ij}[n]))) > 0.5 \\ 0, & else \end{cases} \tag{39}$$

As we can see, SCM directly combines the linking term and the feedback term into an single equation to form an internal activity item U_{ij}.

2.3.4 Feature-Linking Model (FLM)

Compared with SCM, the feature-linking model (FLM) retains feeding wave and linking wave, while reducing parameters. In addition, an inhibition-linking item is contained in FLM. According to [115], FLM can be described as follows,

$$\begin{aligned} U_{ij}[n] =& fU_{ij}[n-1] + \left(\sum_{kl} M_{kl}Y_{kl}[n-1] + S_{ij}\right) \\ & \times\left(1 + \beta\left(\sum_{kl} M_{kl}Y_{kl}[n-1] - d\right)\right) \\ E_{ij}[n] =& gE_{ij}[n-1] + V_E Y_{ij}[n-1] \\ Y_{ij}[n] =& \begin{cases} 1, & if \quad U_{ij}[n] > E_{ij}[n] \\ 0, & else \end{cases} \end{aligned} \tag{40}$$

where f, g denote the attenuation time constant and d is a positive constant for the globally inhibitory.

2.3.5 Improved PCNN Based Enhancement

As mentioned above, based on the mechanism of human visual characteristics, the time matrix of PCNN can be used as an image enhancement tool. In implementation, the enhancement image can be obtained by the negative of the time matrix. Generally, image enhancement algorithms based on time matrix can be summarized as follows:

Step 1: Normalize the image intensity I by:

$$S = \frac{I - \min(I)}{\max(I) - \min(I)} + \varepsilon \tag{41}$$

where $min(I)$ is the minimum value of I and $max(I)$ is the maximum value of I. ε is a small positive value, which is just to avoid zero value in the image.
Step 2: Obtain the time matrix T_{ij} by Algorithm 2.
Step 3: According to the definition of the time matrix, it can be found that the neuron corresponding to the pixels with higher intensity fires earlier than the neuron with a low stimulation. In other words, the neural network receives the higher intensity pixel input in the image and returns a smaller value in the time matrix. Thus, the values in the time matrix need to be reversed. Zhan et al. [115] gave the transformation function as follows:

$$\mathcal{T}_{ij} = \max(T_{ij}) + 1 - T_{ij} \tag{42}$$

Step 4: Normalize $\mathcal{T}_{ij}$ and round to the nearest integer, obtaining the enhanced image $\mathcal{J}$.

$$\mathcal{J} = \left\lfloor 255 \frac{\mathcal{T} - \min(\mathcal{T})}{\max(\mathcal{T}) - \min(\mathcal{T})} + 0.5 \right\rfloor \tag{43}$$

In addition to the above enhancement algorithm, Zhan et al. [116] proposed a linking synaptic computation network (LSCN) and applied it to image enhancement. They considered the gamma band oscillations in visual cortical neurons as the key role to improve the model.

2.4 Rybak Model

Rybak model was derived from the visual cortex system of guinea pigs, and its core structure is the iso-orientation domain model. According to [94, 117], basic Rybak model is proposed based on the screen-type neuron-like structure (SNS) and is described as follows:

$$X_{ij}^S = F^S \otimes \left\| S_{ij} \right\| \tag{44}$$

$$X_{ij}^I = F^I \otimes \left\| Z_{ij} \right\| \tag{45}$$

$$Z_{ij} = f\left\{ \sum X_{ij}^S - (\frac{1}{\phi}) X_{ij}^I - h \right\} \tag{46}$$

where $\otimes$ is the convolution operator. ϕ denotes the time constants of inertial block and h represents the threshold of summarizing element. Obviously, the neuron (i, j) receives stimulus input S_{ij} to form a linking input block X_{ij}^S. F^S is a local connection of "on-center/off-surround" and F^I is a local oriented connection, which exist in the visual cortex neural networks with a large number of different resolutions. In (46), f is a nonlinear threshold function. It can be seen from (44) to (46), Rybak model mainly consists of two parts: feeding input X_{ij} and output Z_{ij}.The algorithmic structure of SNS is shown in Fig. 9.

In Rybak's theory, F^S is defined as a local connection. The input receptive field F^S can enhance the sharp edge information of images [118] and connection receptive field F^I with different forms of orientation connection has a key role in the orientation tuning response of image processing.

2.4.1 Rybak Neural Network (RYNN)

Based on Rybak's theory, Qi et al. [119] proposed a RYNN model by introducing the redefined threshold segmentation module and a nonlinear generator. RYNN's discrete expressions as follows:

$$\begin{cases} E_{ij}[n] = e^{-\alpha_e} E_{ij}[n-1] + V_E Z_{ij}[n-1] \\ X_{Iij}[n] = \alpha \sum_{kl} F_{ijkl}^I Z[n-1] + S_{ij} \\ X_{Sij}[n] = V_S \sum_{kl} F_{ijkl}^S S_{ij} \\ P_{ij}[n] \ = X_{Sij}[n] - \frac{1}{\phi} X_{Iij}[n] + h \\ Z_{ij}(n) = f(P, E) \end{cases} \tag{47}$$

where E_{ij} is dynamic threshold, which is similar as PCNN. f is a nonlinear generator and n is the number of iterations. Other parameters have the same meaning as the basic Rybak model. In Qi et al.'s work, input receptive field F_{ijkl}^S is refined as follows:

$$\begin{aligned} F^S(x, y) &= a_1 \sqrt{x^2 + y^2} \exp(-\frac{x^2 + y^2}{c_1}) \\ &- a_2 \sqrt{x^2 + y^2} \exp(-\frac{x^2 + y^2}{c_2}) \end{aligned} \tag{48}$$

where a_1 and a_2 are the distribution sensitivity. c_1 and c_2 are the spatial distribution of the excitement intensity and inhibitory intensity of the receptive field respectively. The receptive field $F^S(x, y)$ has been proved to have multi-scale adjustable characteristic, which is sensitive to the detailed texture information of the image.

2.4.2 Heterogeneous Rybak neural network (HRYNN)

As we know, Rybak neural networks are analogous to the components of actual neurons. However, lots of researches [120, 121] have shown that the visual cortex system of mammals is heterogeneous. Motivated by this fact, Qi et al. [119] proposed a heterogeneous Rybak neural network (HRYNN) as shown in Fig. 10.

In Qi et al.'s work, HRYNN is described as follows:

$$X_{Sij}[n] = V_S \sum_{kl} F^S_{ijkl} S_{ij} \tag{49}$$

$$X^I_m[n] = \alpha \sum_{kl} F^I_{m,kl} Z_m[n-1] + S_{ij} \quad (m = 1, 2, 3) \tag{50}$$

$$E_{m,ij}[n] = e^{-\alpha_e} E_{m,ij}[n-1] + V_E Z_{m,ij}[n-1] \quad (m = 1, 2, 3) \tag{51}$$

$$P_1[n] = X^S_{ij}[n] - \frac{1}{\phi} X^I_1[n] + h \tag{52}$$

$$P_2[n] = X^S_{ij}[n] - \frac{1}{\phi} X^I_2[n] + h + L_{12} \tag{53}$$

$$P_3[n] = X^S_{ij}[n] - \frac{1}{\phi} X^I_3[n] + h + L_{23} \tag{54}$$

$$Z_{m,ij}[n] = \begin{cases} k_m, & if\ P_{m,ij}[n] > E_{m,ij}[n-1] \\ 0, & else \end{cases} \quad (m = 1, 2, 3) \tag{55}$$

$$Z = Z_1 + Z_2 + Z_3 \tag{56}$$

where m denotes m-th RYNN subcell. It can be seen that the output of HRYNN represents the multi-region processing of the image. Furthermore, the setting of parameters of HRYNN is described as follows [119]:

As shown in Fig. 10, L_{12} and L_{23} are weak connections among different sub-cells of HRYNN. In the work of Qi et al., the linking item L_{12} of RYNN1 and RYNN2 is set as follows:

$$L_{12} = \beta_{12} \sum W_{ijkl}(1,2) Z_{1,kl}(n-1) \tag{57}$$

where β_{12} is the local linking item between RYNN1 and RYNN2: $\beta_{12} = max(I)/mean(I)$. Similarly, L_{23} is set to:

$$L_{23} = \beta_{23} \sum W_{ijkl}(2,3) Z_{2,kl}(n-1) \tag{58}$$

Where β_{23} is the local linking item between RYNN2 and RYNN3: $\beta_{23} = mean(I)/max(I)$. I is the input image. In addition, $W(1, 2)$ and $W(2, 3)$ are weak linking synaptic weight and set as follows:

$$W_{ijkl}(1,2) = W_{ijkl}(2,3) = \frac{1}{(i-k)^2 + (j-l)^2} \tag{59}$$

The parameter α_e is the exponential decay coefficient of dynamic threshold E. F^I_m(m = 1,2,3) represent the orientation connection of 30°, 90° and 120°, respectively, which detect input stimuli in different directions. Inaddition, $k_1 \neq k_2 \neq k_3$ and $k_1, k_2, k_3 \in (0, 1)$.

Algorithm 3: Enhancement by HRYNN model.

Input : The gray image S_{ij}
Output: The enhancement result Y for each image.

```
Initial the parameters of the HRYNN model.
Calculate F^S_{ijkl} according to (47),
calculate L_12 and L_23 according to (56), (57),
respectively.
n = 0.
while n < N do
    n = n + 1
    update E_ij by (31).
    reapt.
    update P_m, Z_m according to (50)-(53), (54)
    calculate Z by (54), calculate EnI_ij by (32).
    Y_0 = EnI_ij · Z
    if any(Z(:)) == 0
        break;
    end
end while
Normalize linearly to obtain Y.
```

Finally, the main steps of HRYNN algorithm for image enhancement is shown in Algorithm 3. In addition, some examples of image enhancement based on PCNN, SCM, FLM, LSCN and HRYNN are presented in Fig. 11. We can see that the edge detail enhancement effect of HRYNN is obviously better than other methods. This is because its receptive field has been specially set. In particular, FLM causes a bad effect on image details preservation.

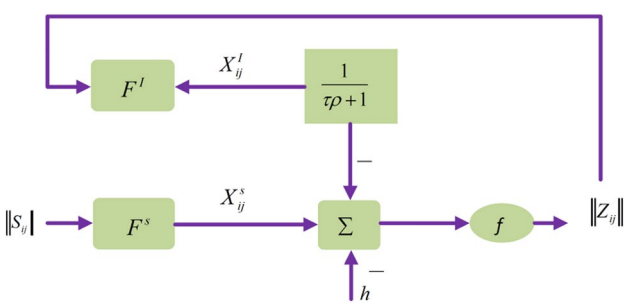

Fig. 9 (i, j)-th Rybak neuron-like element of the SNS

2.5 Deep Learning Based Image Enhancement

In recent years, with the development of artificial intelligence (AI) technology, deep learning has been widely applied in the field of image processing [122–124]. The supervised deep learning based image enhancement methods have great limitations. For each training set, a model must be retrained, which is not universal. Therefore, some researchers began to work on weakly supervised or unsupervised deep learning methods for low-light image enhancement. In this section, for low-light image enhancement, semi-supervised or unsupervised deep learning methods are surveyed in detail.

2.5.1 GAN-Like Based Image Enhancement

Generative Adversarial Network (GAN) is a deep learning model and one of the most promising methods for unsupervised learning on complex distributions in recent years. Here we conduct a review for GAN-like based image enhancement.

In 2018, Ignatov et al. [125] proposed a Weakly Supervised Photo Enhancer (WESPE) for low-light image enhancement based on Generative Adversarial Network (GAN). In their work, the input data and output data are low-quality images and high-quality images, respectively. However, they do not need to correspond in content. In addition, a transitive CNN-GAN structure is used to learn the mapping relationship between them. Two components: generator G and inverse generator F are the main modules of the entire WEPSE model. x is the input low-end image and the improved image $\tilde{y} = G(x)$ is generated through G. A reconstructed low-end image is obtained through the inverse-generator F. The content loss $\mathcal{L}_{content}$ based on vgg-19 is defined between the original and reconstructed images x, and $\tilde{x} = F(\tilde{y}) = F \circ G(x)$, respectively. In addition, adversarial color loss $\mathcal{L}_{color}$ is defined to compare enhanced image and high-quality image. D_c and D_t are two adversarial discriminators, which involve the comparison of color and texture between the enhanced image and the high-quality image respectively. According to [125], $\mathcal{L}_{content}$, $\mathcal{L}_{color}$ and $\mathcal{L}_{texture}$ are defined as follows:

$$\mathcal{L}_{content} = \frac{1}{C_j H_j W_j} \left\| \Psi_j(x) - \Psi_j(\tilde{x}) \right\| \tag{60}$$

$$\mathcal{L}_{color} = -\sum_i \log D_c(G(x)_b) \tag{61}$$

$$\mathcal{L}_{texture} = -\sum_i \log D_t(G(x)_g) \tag{62}$$

where Ψ_j denotes the feature map from j-th VGG-19 convolutional layer. C_j, H_j and W_j are the number, height and width of the feature maps, respectively. A total variation (TV) loss is also defined to impose spatial smoothness of the generated images [126] and its expression is described as follows,

$$\mathcal{L}_{tv} = \frac{1}{CHW} \left\| \nabla_x G(x) + \nabla_y G(x) \right\| \tag{63}$$

where C, H and W are dimensions of the generated image $G(x)$. Finally, WESPE loss is defined as the linear weighting of the four component losses.

Chen et al. [127] proposed a unpaired learning method based on GAN. In their method, two-way generative adversarial networks (GANs) with improvement are employed as the baseline. In addition, U-Net with global feature is use as the generator of GAN model and an adaptive weighting scheme is proposed to improve Wasserstein GAN (WGAN), training converges faster and better. Finally, to make generators better adapt to their own input distributions, they proposed to use the individual batch normalization layers in the two-way GANs model. Although Chen et al. [127]'s method has the advantages of stable performance, fast speed, and outstanding effects for image enhancement, it also has many potential shortcomings. If the input image is very dark and contains a lot of noise, the noise may be amplified in the enhanced image. For unpaired network training, the choice of domain of the training set has great limitations. For the exterior scenes in the paper, lots of images of blue sky and sea were selected. If we do not choose to use, the enhanced images will appear blue for unknown reasons.

Jiang et al. [128] proposed an EnlightenGAN method for deep light enhancement. EnlightenGAN uses attention-guided U-Net as a generator, and uses dual discriminators (global and local) to balance global and local low-light enhancement. In addition, due to the lack of ground truth, the paper proposes an adaptive perceptual loss including global and local to constrain the feature difference between

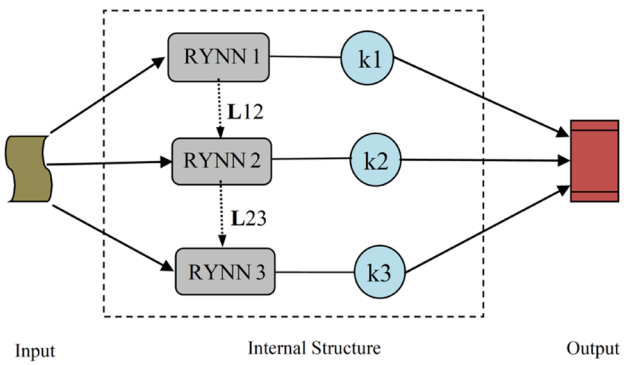

Fig. 10 The architecture of HRYNN

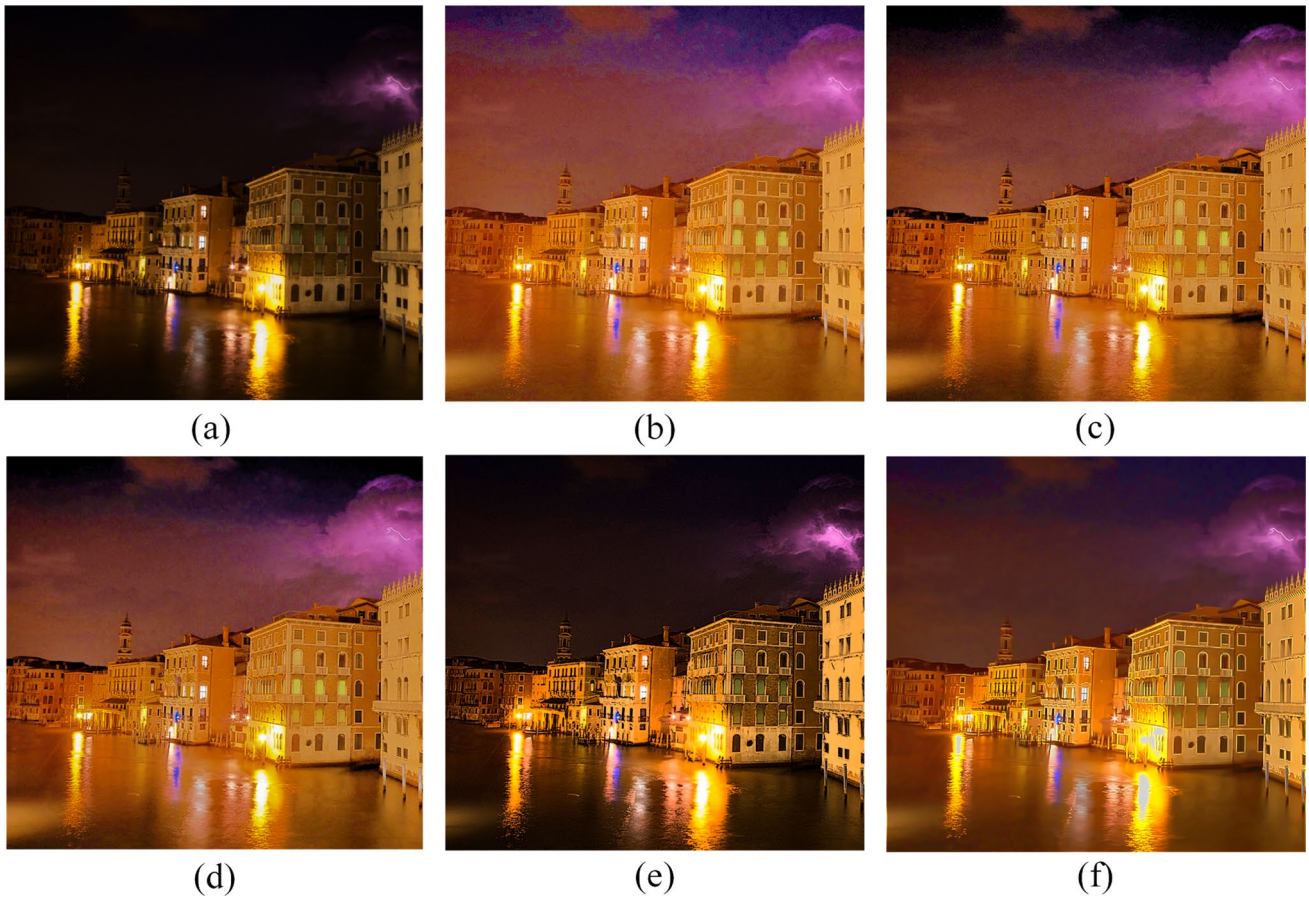

Fig. 11 Some examples of image enhancement. **a** is the original image. **b–f** are the enhancement results by PCNN, SCM, FLM, LSCN and HRYNN, respectively

the low-light input image and its enhanced image, and together with the adversarial loss used to train EnlightenGAN to form the final loss. Furthermore, Xiong et al. [129] proposed a full unsupervised method for real-world low-light image enhancement based on the two-stage GAN frame.

2.5.2 Other Weakly Supervised Methods

In addition to the unsupervised image enhancement methods mentioned above, In this section, we will mainly introduce several weakly-supervised enhancement methods for low-light enhancement.

Yang et al. [130] proposed a semi-supervised method for low-light image enhancement. In their work, firstly, supervised learning is employed to obtain the characteristics of reconstructed high-quality images. Then these characteristics are used as the intermediate variables to assist unsupervised training. In 2019, Shin et al. [131] proposed a novel deep learning method for power-constrained contrast enhancement (PCCE). They constrain the power consumption by reducing the brightness and the perceived visual quality is preserved by CNN enhancement.

In summary, most of unsupervised methods usually use some indirect training methods, such as supervised methods to obtain high-quality image features, and then assist unsupervised training based on these features. In the future, generative adversarial network (GAN) may be widely used in unsupervised image enhancement. This can be better optimized by combining some essential attributes of the image such as retinex and low rank, etc.

3 Supervised Methods

For image enhancement, supervised methods of image enhancement are usually trained based on paired dataset and achieve a good effect. In recent years, a large number of supervised enhancement methods have emerged, such as fully convolutional networks (FCN) [132, 133], reinforcement learning [134–136] and U-Net [137], etc.

In this section, we mainly focus on a detailed overview of supervised deep learning methods for low-light image enhancement.

3.1 Multi-Level Features Fusion Methods

As we know, low-quality images often exhibit low contrast, artifacts, and noise due to some extreme conditions. Based on the excellent feature extraction capabilities of deep convolutional neural networks, many methods for low-brightness image enhancement based on multi-level features fusion have emerged. Here we will give a brief overview of low-brightness image enhancement methods based on multi-level features fusion.

Gharbi et al. [138] proposed a deep bilateral learning based enhancement method with the idea of multi-level features fusion. In their work, Three main strategies are proposed to fuse features of different levels to effectively enhance low-brightness images. Firstly, most of the predictions are performed under a low-resolution bilateral grid; Secondly, the entire neural network structure learns an affine transformation; Thirdly, most of the operations are performed at low resolution, but the loss function is finally established on the original resolution, in other words, the original resolution image can be optimized based on low resolution operations. In 2018, Lv et al. [139] proposed a multi-branch low-light enhancement network (MBLLEN). They employed the multiple subnets to extract different level features and finally conducted a multi-branch fusion, achieving an outstanding enhancement effect. In addition, Cai et al. [140] proposed a single image enhancement method based on multi-exposure image fusion. However, if the input image is severely overexposed and the area is large, CNN can use little neighborhood information. Thus, it is difficult to synthesize these missing details. Lv et al. [141] designed a multi-branch fusion network guided by the attention map, which can perform image denoising and enhancement simultaneously. Zamir et al. [142] proposed a MIRNet model, which executes parallel resolution convolution streams to extract multi-scale features and exchanges information across resolution streams. Finally, attention-based multi-scale feature aggregation is proposed for image enhancement. In addition, similar work was also conducted by Zhu et al. [143].

In conclusion, the image enhancement methods based on multi-level features fusion fully take into account the importance of different scale features of the image for image restoration. For example, high-frequency features determine the preservation of the details of the image, while low-frequency features play a key role in preserving the naturalness of the image. Therefore, multi-level features fusion is an effective method in the enhancement of low-light images.

3.2 Retinex-Based Deep Learning Methods

In Sect. 2.2, we have mentioned that Retinex theory plays an important role in image enhancement applications. The Retinex model is the basic theory of human visual imaging, and increasing researchers are beginning to work on its combination with deep learning for image enhancement [144]. Shen et al. [145] thought that the traditional multi-scale Retinex (MSR) [63] algorithm can be regarded as a feedforward convolutional neural network with different Gaussian convolution kernels. Therefore, they proposed MSR-net to directly learn end-to-end enhanced mapping. MSR-net consists of three modules: multi-scale logarithmic transformation, convolution difference and color restoration. In addition, the training data uses high-quality images adjusted by PS and corresponding synthetic low-light images (randomly reduced brightness, contrast, and gamma correction). The loss function is the F-norm square of the error matrix with regular terms.

In 2018, Li et al. [14] proposed a LightenNet for low light image enhancement, which only learns to predict the mapping relations between weakly illuminated image and the corresponding illumination map of Retinex model. Although their method has the advantages of easy training and short time-consuming, it shows great limitations in enhancing low-quality images with noise, because the training set only uses high-quality images. Wei et al. [146] proposed a deep Retinex-Net, including a Decom-Net for decomposition and an Enhance-Net for illumination adjustment. In their work, a low-light dataset (LOL) containing low/normal-light image pairs was collected. In addition, Shi et al. [147] combined the Retinex model and the Generative Adversarial Network (GAN) to enhance low-light images. Specifically, the decomposition part divides the image into a illumination image and reflected image, and the enhancement part is used to generate a high-quality image.

Noise is an interference factor that must be considered in low-brightness image enhancement. Inspired by this fact, many scholars have proposed noise suppression low-brightness image enhancement methods based on the Retinex model. Wang et al. [148] considered that contrast enhancement and noise removal are coupled problems, proposing a novel progressive Retinex framework, which makes illumination and noise of low-light image be perceived in a mutually reinforced manner, achieving noise reduction low-light enhancement results. However, Wang et al.'s method has a limitation. Because it only considers the statistical distribution of the pixel space and ignores the structural properties. In addition, the receptive field of the 1×1 convolution kernel is relatively small, resulting in no neighborhood information during convolution. Liang et al. [149] proposed a deep learning method for low-light images enhancement. Their methods particularly

focused on measurement noise. Specially, a neural network is trained to generated a set of pixel-wise operators, which can simultaneously predict the noise and the illumination layer in the bilateral space.

3.3 HDR Image Reconstruction

In general, camera sensors can only capture images with a limited range of lightness and a high dynamic range (HDR) image, in practice, is necessary. Therefore, many researches focus on predicting its saturated pixel value for the reconstruction of HDR images. In 2017, Gaberiel et al. [150] proposed a deep convolutional neural network (CNN) to predict the HDR values of images. In Gaberiel et al.'s work, a large dataset of HDR images is collected to train CNN. In particular, these datas are augmented by simulating the sensor saturation of a series of cameras. Yang et al. [151] proposed a Deep Reciprocating HDR Transformation (DRHT). In their work, the missing details in the HDR domain firstly are reconstructed. Then, the LDR image with the recovered details is generated by performing tone mapping on the predicted HDR data. Therefore, their method framework mainly consists of two parts: HDR reconstruction and tone mapping.

4 Quality Evaluation

The quality evaluation of image processing algorithms is essential, which involve people's evaluation of the visual perception of an image. In image enhancement, an appropriate quality evaluation strategy plays a key role in the evaluation of algorithm performance. In this section, we will give a detailed overview of the qualitative and quantitative evaluation for image enhancement.

4.1 Qualitative Assessment

It is difficult to quantify an improved perception of an image. Therefore, it is not easy to assess image enhancement [152]. But in general, it is desirable to conduct both quantitative and qualitative assessments. Qualitative evaluation refers to intuitively expressing people's visual perception of enhanced images, and is the most accurate evaluation method. However, subjective evaluation methods lack stability. It is often affected by various factors such as experimental conditions, the observer's knowledge background, mood, motivation, and fatigue.

In this section, we will conduct a comprehensive and systematic experimental evaluation of image enhancement methods. The methods involved mainly include the following representative methods: histogram equalization, Retinex-based enhancement and visual cortical neural network. The experimental evaluation of deep learning-based methods will be presented in Sect. 4.2 in the form of quantitative comparison. In addition, due to the limitation of the paper length, here we only perform experimental evaluations of representative methods for each image enhancement type. Detailed experimental settings, which can be found in the original papers, are missed. We compare various image enhancement methods on randomly selected low-brightness test images. The evaluated approaches include Histogram Equalization (HE), Adaptive Histogram Equalization (AHE), partially overlapped sub-block histogram equalization(POSHE) [27], WTHE [29] and AGCWD [33], SRIE [85], LIME [86], SCM [113] and HRYNN [119]. A example of visual comparison based on different image enhancement is shown in Fig. 12.

We can see from Fig. 12 that AHE and SRIE have better performance in detail enhancement, but HE, WTHE and AGCWD cause serious loss of details, such as the edge of a teacup, etc. Obviously, HRYNN has the best detail preservation performance, as marked by red boxes. In addition, SCM seems to have an artifact effect and LIME cause a illumination over-enhancement, which adds to the noise amplification. AHE and AGCWD cannot achieve satisfactory results in overall contrast, such as a low contrast of flowers etc.

In summary, the histogram equalization enhancement is based on the fact that it represents the statistical relationship between each gray level in the image and the number of pixels that appear in the gray level, and reflects the frequency of each gray level in the image. In practice, histogram equalization still has certain limitations. It is usually necessary to consider combining a variety of simple and effective algorithms, or fusing other enhancement techniques to achieve the final enhancement effect, so comprehensive image enhancement technology will also become a the key of follow-up study. Retinex model assumes that image lightness depends on illumination and re ectance. Illumination is the radiant flux received by the scene, and reflectivity is the effectiveness of reflected radiant energy. In addition, the perception of color has a strong correlation with reflectivity [47]. Finally, the visual cortex neural network is based on the principle of human visual characteristics and has great potential in the field of image enhancement.

4.2 Quantitative Assessment

The quantitative assessment method adopts the error between the processed image and the original image to measure the quality of the processed image. Specifically, the greater the grayscale difference from the standard image, the more severe the image quality degradation. Representative

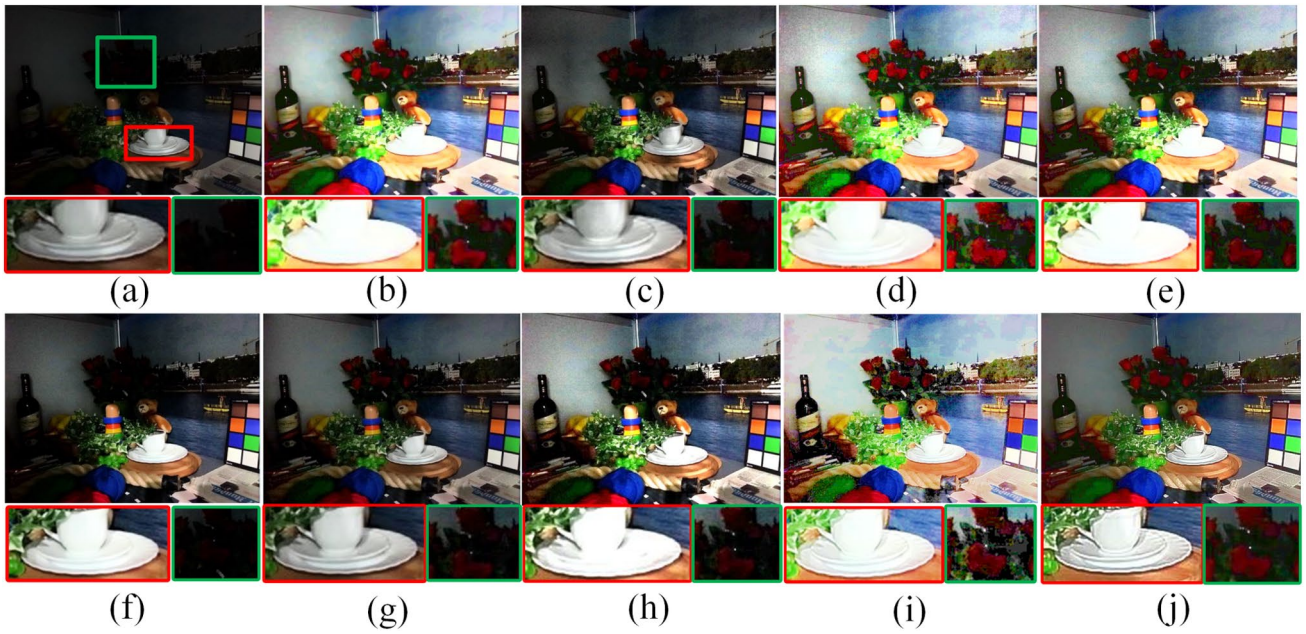

Fig. 12 Visual comparison of different image enhancement based on HE-like methods. **a** is the original image. Enhanced images generated by: **b** HE; **c** AHE; **d** POSHE; **e** WTHE; **f** AGCWD; **g** SRIE; **h** LIME; **i** SCM; **j** HRYNN

methods include mean square error (MSE) and peak signal-to-noise ratio (PSNR). In this section, we first elaborates the quantitative evaluation index for the enhanced image. Then, the experimental evaluation of deep learning based image enhancement methods is conducted.

4.2.1 Quantitative Index

The quantitative measures we introduced here mainly involve absolute mean brightness error (AMBE) [153], structural similarity of image (SSIM) [154] and peak signal to noise ratio (PSNR), discrete entropy (DE) [155], enhancement (EME) [156] and lightness order error (LOE) [157].

First of all, according to literature [153], the absolute mean brightness error(AMBE) is defined as:

$$AMBE(X, Y) = |MB(X) - MB(Y)| \tag{64}$$

where *MB(X)* and *MB(Y)* represent the mean brightness of original image *X* and enhanced image *Y*, respectively. In addition, the lower the value AMBE the better is preservation of the original image luminance.

Then, structural similarity of image (SSIM) is used to evaluate the similarity of two images and is proposed by Wang et al. [154]. It is usually described as follows:

$$SSIM(x, y) = l(x, y)^{\alpha} \cdot c(x, y)^{\beta} \cdot s(x, y)^{\gamma} \tag{65}$$

where $l(x, y)$, $c(x, y)$ and $s(x, y)$ denote brightness comparison part, contrast comparison part and structure comparison part of image, respectively. In addition, α, β and γ are parameters employed to adjust the relative importance of the three components. Generally, they are set to 1 and related parameters are defined as follows:

$$\begin{aligned} l(x, y) &= \frac{2\mu_x\mu_y + c_1}{\mu_x^2 + \mu_y^2 + c_1}, \quad c(x, y) = \frac{2\sigma_x\sigma_y + c_2}{\sigma_x^2 + \sigma_y^2 + c_2}, \\ s(x, y) &= \frac{\sigma_{xy} + c_3}{\sigma_x\sigma_y + c_3} \end{aligned} \tag{66}$$

where x and y represent the original image and enhanced image, respectively. μ_x, μ_y, σ_x^2, σ_y^2 and σ_{xy} denote the mean, variance and covariance of image x and y respectively. In addition, c_1, c_2 and c_3 are small constants, just to avoid the fact that the denominator is zero. The larger the value of SSIM, it means that the structure of the enhanced image is similar to the original image and the quality of the enhanced image is better. Note SSIM(x,y) $\in$ (0,1).

Peak signal-to-noise ratio (PSNR) is usually employed to roughly estimate the human perception of reconstruction quality [158]. PSNR is calculated as follows:

$$PSNR = 10\log_{10}\left(\frac{peakval^2}{MSE}\right) \tag{67}$$

where *peakval* is the maximal variation of the input image data. If it has an 8-bit unsigned integer data type, *peakval* is 255. In addition, *MSE* represent the mean square error of input image I and enhanced image I_0 with resolution $m \times n$:

$$MSE = \frac{1}{mn}\sum_{i=0}^{m-1}\sum_{j=0}^{n-1}\left\|I(i,j) - I_0(i,j)\right\|^2 \tag{68}$$

The discrete entropy (DE) of an image X is

$$DE(X) = -\sum_{i=0}^{255} p(x_i)\log p(x_i) \tag{69}$$

where $p(x_i)$ is the probability of pixel intensity x_i, which is estimated from the normalized histogram. A higher value of DE indicates the image has richer details.

If we divide the image X into k_1k_2 non-overlapping sub-blocks X_{ij} with size $\omega_1 \times \omega_2$. Then EME can be computed as

$$EME(X) = \frac{1}{k_1k_2}\sum_{i=1}^{k_1}\sum_{j=1}^{k_2} 20In\frac{\max(X_{ij})}{\min(X_{ij})} \tag{70}$$

where $\max(X_{ij})$ and $\min(X_{ij})$ represent the maximum and minimum grey levels in block X_{ij}, respectively. A different sub-block size (ie., $\omega_1 \times \omega_2$) will result in different EME value. High contrast sub-blocks give a high EME value and the homogeneous sub-blocks can result in an EME value close to 0. Note that EME is highly sensitive to noise. Specifically, if the algorithm generates an output image, which introduces noise over homogeneous regions of the image, then although the output image looks unnatural, its corresponding EME value is very high [152].

Finally, the lightness order error (LOE) is of great significance for describing the naturalness of the image, which is proposed to evaluate the quality of the image. If I represents the original image and I_e represents the enhanced image, the lightness of the image is represented by the highest brightness among the three channels:

$$L(x,y) = \max_{c\in\{r,g,b\}} I^c(x,y) \tag{71}$$

For each pixel, before and after image enhancement, the lightness order error related to that pixel is defined as follows:

$$RD(x,y) = \sum_{i=1}^{m}\sum_{j=1}^{n}\left(U(L(x,y),L(i,j)) \oplus U(L_e(x,y),L_e(i,j))\right) \tag{72}$$

where m and n represent the height and width of the image respectively. $U(x, y)$ is step functions, and $\oplus$ represent the exclusive OR operation. Thus, LOE is defined as follows:

$$LOE = \frac{1}{m*n}\sum_{i=1}^{m}\sum_{j=1}^{m} RD(i,j). \tag{73}$$

Due to the large amount of calculation of the LOE algorithm, in practical applications, the image is generally downsampled with a sampling rate of $50/\min(m,n)$ to achieve the purpose of reducing the amount of calculation. It can be seen from equation (73) that the smaller the LOE value, the higher the naturalness of the image and the higher the quality.

Due to the limitation of the paper length, we only elaborated the detailed algorithm of the above image quality evaluation indicators. There are some other evaluation indicators, such as average brightness (AB) [159], visual information fidelity (VIF) [160], tone mapped image quality index (TMQI) [161] and learned perceptual image patch similarity metric (LPIPS) [162]. Detailed algorithm content, which can be found in the original papers, are missed.

4.2.2 Experimental Evaluation

In this section, we compare various image enhancement methods on synthetic dataset (SYD) [141]. SYD is a large scale low-light simulation dataset with 22,656 scenes, which has diverse scenes and lighting conditions. In quantitative comparison, some indicators such as PSNR, SSIM [154], average brightness (AB) [159], visual information fidelity (VIF) [160], lightness order error (LOE) [157], tone mapped image quality index (TMQI) [161] and learned perceptual image patch similarity metric (LPIPS) [162] are employed to evaluate the representative low-lightness image enhancement methods we investigated. All the results are from the original paper, and they are recorded in Table 1. Note that implementation is done with Keras and Tensorflow.

The evaluated image enhancement methods cover BIMEF [164], LIME [86], MSRCR [10], MF [163], SRIE [85], Dong [165], NPE [157] , DHECI [166], BPDHE [40], HE, Ying [168], WAHE [31], JED [167], Robust [87], LLNet [171], DeepUPE [169], GLADNet [170], MBLLEN [139] and Lv [141]. Note that in the Table 1 below, blod and underlined indicate the best and second place results, respectively. We can see from Table 1 that Lv et al. [141] achieved the best overall performance. In their work, a multi-branch network with a ue-attention map and noise map was proposed to enhancement low light images in a region adaptive manner. In addition, supervised methods such as LLNet [171], DeepUPE [169], GLADNet [170], MBLLEN [139] and Lv [141] basically achieved a better performance. For example, their metric SSIM reach above 0.6. It is worth noting that JED [167] and Robust [87] require a lot of computing resources, which can cause insufficient memory when processing large images.

Table 1 Quantitative comparison of synthetic low-light image data sets (without additional noise) enhanced. Bold and underlined indicate the best and second place results, respectively. "↑" means higher is better, "↓" means lower is better, "⇓" means lower absolute value is better

	PSNR ↑	SSIM ↑	LPIPS ↓	VIF ↑	LOE ↓	TMQI ↑	AB ⇓
Input	11.99	0.45	0.26	0.33	677.85	0.80	– 59.22
MF [163]	15.89	0.68	0.18	0.44	766.00	0.83	– 36.88
MSRCR [10]	14.87	0.72	0.15	0.52	1249.24	0.82	35.07
SRIE [85]	13.83	0.56	0.21	0.37	787.42	0.82	– 47.86
BIMEF [164]	18.28	0.76	0.11	0.49	550.20	0.85	– 28.06
NPE [157]	14.93	0.66	0.18	0.42	875.15	0.83	– 41.35
LIME [86]	15.80	0.68	0.20	0.48	1121.17	0.80	<u>– 2.46</u>
Dong [165]	15.37	0.65	0.22	0.35	1228.49	0.81	– 33.80
DHECI [166]	18.13	0.76	0.17	0.39	547.12	0.87	– 17.37
BPDHE [40]	13.62	0.60	0.24	0.34	609.89	0.82	-47.82
MBLLEN [139]	24.21	<u>0.90</u>	**0.08**	<u>0.63</u>	536.75	<u>0.91</u>	– 3.66
Lv [141]	**25.24**	**0.94**	**0.08**	**0.67**	**495.48**	**0.93**	**2.04**
WAHE [31]	15.46	0.65	0.18	0.44	564.83	0.84	– 39.38
JED [167]	16.11	0.65	0.21	0.41	1212.66	0.82	– 25.95
Robust [87]	16.83	0.69	0.20	0.47	1052.22	0.82	– 22.09
HE	17.88	0.76	0.18	0.47	596.67	0.88	19.24
Ying [168]	19.21	0.80	0.11	0.56	778.67	0.83	– 9.28
DeepUPE [169]	16.55	0.64	0.17	0.55	516.47	0.84	– 30.48
GLADNet [170]	<u>24.57</u>	<u>0.90</u>	<u>0.09</u>	0.62	<u>513.18</u>	<u>0.91</u>	5.52
LLNet [171]	20.11	0.80	0.39	0.40	1088.43	0.87	4.30

From these results, we can draw the conclusion that deep learning-based methods are in the leading position. The performance can be improved by the following strategies: designing novel optimization loss, modifying channel attention mechanism, Retinex combination, adapting scale-aware enhancement, and learning multi-level fused CNN features.

5 Conclusion

Image enhancement plays important roles in image processing. In this paper, we give a comprehensive review to analyze image enhancement methods from a supervised and unsupervised perspective. There are three main aspects. We first survey the unsupervised image enhancement methods, including histogram specification, Retinex model, deep learning and visual cortex neural network. Then we introduce supervised image enhancement methods involving deep convolutional neural network. In addition, we also provide main quality evaluation methods for image enhancement. In the future, weakly supervised or unsupervised strategies will probably generate new image enhancement frameworks and bring a rapid progress than state-of-the-art algorithms.

Acknowledgements This work is jointly supported by the National Natural Science Foundation of China (No.62061023 and 61961037), the Natural Science Foundation of Gansu Province (No.18JR3RA288) and the Fundamental Research Funds for the Central Universities of China (No.lzujbky-2017-it72).

Declarations

Conflict of interest The authors declare that they have no conflict of interest.

References

1. Bedi SS, Khandelwal R (2013) Various image enhancement techniques-a critical review. Int J Adv Res Comput Commun Eng 2(3):1605–1609
2. Walter RJ , Berns MW (1986) Digital Image Processing and Analysis[M]. IEEE Computer Society Pr
3. Chang D, Wu W (1998) Image contrast enhancement based on a histogram transformation of local standard deviation. IEEE Trans Med Imaging 17(4):518–531
4. Wang Y, Chen Q, Zhang B (1999) Image enhancement based on equal area dualistic sub-image histogram equalization method. IEEE Trans Consum Electron 45(1):68–75

5. Agaian SS, Silver B, Panetta KA (2007) Transform coefficient histogram-based image enhancement algorithms using contrast entropy. IEEE Trans Image Process 16(3):741–758
6. Polesel A, Ramponi G, Mathews V (2000) Image enhancement via adaptive unsharp masking. IEEE Trans Image Process 9(3):505–510
7. Lin S, Wong C, Jiang G, Rahman M, Ren T, Kwok N, Shi H, Yu Y-H, Wu T (2016) Intensity and edge based adaptive unsharp masking filter for color image enhancement. Optik Int J Light Electron Opti 27(1):407–414
8. Liu L, Jia Z, Yang J, Kasabov N (2015) A medical image enhancement method using adaptive thresholding in nsct domain combined unsharp masking. Int J Imaging Syst Technol 25(3):199–205
9. Jobson D, Rahman Z (1997) Properties and performance of a center/surround retinex. IEEE Trans Image Process A Publ IEEE Signal Process Soc 6(3):451–462
10. Jobson DJ, Rahman Z, Woodell GA (2002) A multiscale retinex for bridging the gap between color images and the human observation of scenes. IEEE Trans Image Process 6(7):965–976
11. Rahman Z, Jobson DJ, Woodell GA (2004) Retinex processing for automatic image enhancement. J Electron Imaging 13(1):100–110
12. Zhengang S, Liqun G, Kun W (2007) A novel approach to image enhancement and thresholding based on fuzzy theory. In: IEEE Conference on industrial electronics and applications 2201–2205
13. Kong XW (2007) The fuzzy image enhancement algorithm for iow snr image. Laser J 5:44–45
14. Li C, Guo J, Porikli F, Pang Y (2018) Lightennet: a convolutional neural network for weakly illuminated image enhancement. Pattern Recognit Lett 104:15–22
15. Zheng WT, Pu T, Cheng J, Zheng H (2012) Image contrast enhancement by contourlet transform and pcnn, In: International conference on audio, language and image processing 735–739
16. Singh GMA (2014) Various image enhancement techniques-a critical review. Int J Innov Sci Res 10(2):267–274
17. Bahmani B, Moseley B, Vattani A, Kumar R, Vassilvitskii S (2012) Scalable k-means++. Proc Vldb Endow 5(7):622–633
18. D'Andrade RG (1978) U-statistic hierarchical clustering. Psychometrika 43(1):59–67
19. Dempster AP (1977) Maximum likelihood from incomplete data via the em algorithm. J R Stat Soc 39
20. Wang X, Chen L (2017) An effective histogram modification scheme for image contrast enhancement. Signal Process Image Commun 58:187–198
21. Qiuqi R, Yuzhi R (2013) Digital Image Processing, 3rd edn. Publishing House of Electronics Industry
22. Le-Peng LI, Sun SF, Xia C, Chen P, Dong FM (2014) Survey of histogram equalization technology. Comput Syst Appl 03:1–8
23. Zuiderveld K (1994) Contrast limited adaptive histogram equalization. Graphics Gems 474–485
24. Wang Y, Pan Z (2017) Image contrast enhancement using adjacent-blocks-based modification for local histogram equalization. Infrared Phys Technol 86:59–65
25. Lamberti F, Montrucchio B, Sanna A (2006) Cmbfhe: a novel contrast enhancement technique based on cascaded multistep binomial filtering histogram equalization. IEEE Trans Consum Electron 52(3):966–974
26. Liu B, Jin W, Chen Y, Liu C, Li L (2011) Contrast enhancement using non-overlapped sub-blocks and local histogram projection. IEEE Trans Consum Electron 57(2):583–588
27. Kim J, Kim L, Hwang S (2001) An advanced contrast enhancement using partially overlapped sub-block histogram equalization. IEEE Trans Circuits Syst Video Technol 11(4):475–484
28. Agarwal M, Mahajan R (2017) Medical images contrast enhancement using quad weighted histogram equalization with adaptive gama correction and homomorphic filtering. Procedia Comput Sci 115:509–517
29. Wang Q, Ward RK (2007) Fast image/video contrast enhancement based on weighted thresholded histogram equalization. IEEE Trans Consum Electron 53(2):757–764
30. Wong CY, Liu S, Liu SC, Rahman A, Lin SCF, Jiang G, Kwok NM, Shi H (2016) Image contrast enhancement using histogram equalization with maximum intensity coverage. J Modern Opt 63(16):1618–1629
31. Arici T, Dikbas S, Altunbasak Y (2009) A histogram modification framework and its application for image contrast enhancement. IEEE Trans Image Process 18(9):1921–1935
32. Yun SH, Jin HK, Kim S (2011) Contrast enhancement using a weighted histogram equalization. In: IEEE International Conference on Consumer Electronics
33. Huang S, Cheng F, Chiu Y (2013) Efficient contrast enhancement using adaptive gamma correction with weighting distribution. IEEE Trans Image Process 22(3):1032–1041
34. Huang Z, Zhang T, Li Q, Fang H (2016) Adaptive gamma correction based on cumulative histogram for enhancing near-infrared images. Infrared Phys Technol 79:205–215
35. Kim Y (1997) Contrast enhancement using brightness preserving bi-histogram equalization. IEEE Trans Consum Electron 43(1):1–8
36. Der Chen S, Ramli AR (2003) Minimum mean brightness error bi-histogram equalization in contrast enhancement. IEEE Trans Consum Electron 49(4):1310–1319
37. Tan TL, Sim KS, Tso CP (2012) Image enhancement using background brightness preserving histogram equalisation. Electron Lett 48(3):155–157
38. Singh K, Vishwakarma DK, Walia GS, Kapoor R (2016) Contrast enhancement via texture region based histogram equalization. J Modern Opt 63(15):1444–1450
39. Abdullahalwadud M, Kabir H, Dewan MAA, Chae O (2007) A dynamic histogram equalization for image contrast enhancement. IEEE Trans Consum Electron 53(2):593–600
40. Ibrahim H, Kong NSP (2007) Brightness preserving dynamic histogram equalization for image contrast enhancement. IEEE Trans Consum Electron 53(4):1752–1758
41. Zhao W, Xu Z, Zhao J, Zhao F, Han X (2014) Infrared image detail enhancement based on the gradient field specification. Appl Opt 53(19):4141–4149
42. Fu JC, Lien HC, Wong STC (2000) Wavelet-based histogram equalization enhancement of gastric sonogram images. Comput Med Imaging Graph 24(2):59–68
43. Kaur A, Singh C (2017) Contrast enhancement for cephalometric images using wavelet-based modified adaptive histogram equalization. Appl Soft Comput 51:180–191
44. Ooi CH, Kong NSP, Ibrahim H (2009) Bi-histogram equalization with a plateau limit for digital image enhancement. IEEE Trans Consum Electron 55(4):2072–2080
45. Singh K, Kapoor R (2014) Image enhancement via median-mean based sub-image-clipped histogram equalization. Optik 125(17):4646–4651
46. Singh K, Kapoor R (2014) Image enhancement using exposure based sub image histogram equalization. Pattern Recognit Lett 36:10–14
47. Land EH (1977) The retinex theory of color vision. Sci Am 237(6):108–128
48. Land EH, Mccann JJ (1971) Lightness and retinex theory. J Opt Soc Am 61(1):1–11
49. Land EH (1983) Recent advances in retinex theory and some implications for cortical computations: color vision and the natural image. Proc Natl Acad Sci U S Am 80(16):5163–5169

50. Brainard DH, Wandell BA (1986) Analysis of the retinex theory of color vision. J Opt Soc Am A Opt Image Sci Vis 3(10):1651–1661
51. Rizzi A, Gatta C, Marini D (2003) A new algorithm for unsupervised global and local color correction. Pattern Recognit Lett 24(11):1663–1677
52. Provenzi E, De Carli L, Rizzi A, Marini D (2005) Mathematical definition and analysis of the retinex algorithm. J Opt Soc Am A Opt Image Sci Vision 22(12):2613–2621
53. Marini D, Rizzi A (2000) A computational approach to color adaptation effects. Image Vision Comput 18(13):1005–1014
54. Cooper TJ, Baqai FA (2004) Analysis and extensions of the frankle-mccann retinex algorithm. J Electron Imaging 13(1):85–92
55. Gianini G, Lecca M, Rizzi A (2016) A population-based approach to point-sampling spatial color algorithms. J Opt Soc Am A Opt Image Sci Vision 33(12):2396–2413
56. Zosso D, Tran G, Osher S (2015) Non-local retinex-a unifying framework and beyond. Siam J Imaging Sci 8(2):787–826
57. Frankle JA, Mccann JJ (1983) Method and apparatus for lightness imaging
58. Provenzi E, Fierro M, Rizzi A, De Carli L, Gadia D, Marini D (2007) Random spray retinex: a new retinex implementation to investigate the local properties of the model. IEEE Trans Image Process 16(1):162–171
59. Banic N, Loncaric S (2013) Light random sprays retinex: exploiting the noisy illumination estimation. IEEE Signal Process Lett 20(12):1240–1243
60. Banic N, Loncaric S (2015) Smart light random memory sprays retinex: a fast retinex implementation for high-quality brightness adjustment and color correction. J Opt Soc Am A Opt Image Sci Vision 32(11):2136–2147
61. Bertalmio M, Caselles V, Provenzi E (2009) Issues about retinex theory and contrast enhancement. Int J Comput Vision 83(1):101–119
62. Land EH (1986) An alternative technique for the computation of the designator in the retinex theory of color vision. Proc Natl Acad Sci U S Am 83(10):3078–3080
63. Rahman Z, Jobson DJ, Woodell GA (1996) Multi-scale retinex for color image enhancement 3:1003–1006
64. Petro AB, Sbert C, Morel JM (2014) Multiscale retinex. Image Process Line 4:71–88
65. Wang S, Luo G (2018) Naturalness preserved image enhancement using a priori multi-layer lightness statistics. IEEE Trans Image Process 27(2):938–948
66. Provenzi E (2017) Formalizations of the retinex model and its variants with variational principles and partial differential equations. J Electron Imaging 27(1):011003
67. Horn BK (1974) Determining lightness from an image. Comput Graph Image Process 3(4):277–299
68. Blake A (1985) Boundary conditions for lightness computation in Mondrian world. Comput Vis Graph Image Process 32(3):314–327
69. Blake A (1985) On Lightness Computation in Mondrian World, Palgrave Macmillan UK
70. Brelstaff G, Blake A (1987) Computing lightness. Pattern Recognit Lett 5(2):129–138
71. Morel J, Petro AB, Sbert C (2009) Fast implementation of color constancy algorithms. Proc of SPIE 7241:724106
72. Morel J, Petro AB, Sbert C (2010) A pde formalization of retinex theory. IEEE Trans Image Process 19(11):2825–2837
73. Ma W,Morel JM, Osher S, Chien A (2011) An l1-based variational model for retinex theory and its application to medical images, In: The 24th IEEE Conference on Computer Vision and Pattern Recognition, CVPR 2011, Colorado Springs, CO, USA, 20-25 June 2011
74. Osher S, Burger M, Goldfarb D, Xu J, Yin W (2005) An iterative regularization method for total variation-based image restoration. Multiscale Model Simul 4(2):460–489
75. Palmaamestoy R, Provenzi E, Bertalmio M, Caselles V (2009) A perceptually inspired variational framework for color enhancement. IEEE Trans Pattern Anal Mach Intell 31(3):458–474
76. Buchsbaum G (1980) A spatial processor model for object colour perception. J Frankl Inst Eng Appl Math 310(1):1–26
77. Provenzi E, Caselles V (2014) A wavelet perspective on variational perceptually-inspired color enhancement. Int J Comput Vision 106(2):153–171
78. Kimmel R, Elad M, Shaked D, Keshet R, Sobel I (2003) A variational framework for retinex. Int J Comput Vision 52(1):7–23
79. Chen T, Yin W, Zhou XS, Comaniciu D, Huang TS (2006) Total variation models for variable lighting face recognition. IEEE Trans Pattern Anal Mach Intell 28(9):1519–1524
80. Ng MK, Wang W (2011) A total variation model for retinex. Siam J Imaging Sci 4(1):345–365
81. Ma W, Osher S (2012) A tv bregman iterative model of retinex theory. Inverse Probl Imaging 6(4):697–708
82. Rudin L, Osher S, Fatemi E (1992) Nonlinear total variation based noise removal algorithms. Phys D Nonlinear Phenom 60:259–268
83. Fu X, Liao Y, Zeng D, Huang Y, Zhang X, Ding X (2015) A probabilistic method for image enhancement with simultaneous illumination and reflectance estimation. IEEE Trans Image Process 24(12):4965–4977
84. Goldstein T, Osher S (2009) The split bregman method for l1-regularized problems. Siam J Imaging Sci 2(2):323–343
85. Fu X, Zeng D, Huang Y, Zhang X, Ding X (2016) A weighted variational model for simultaneous reflectance and illumination estimation, In: IEEE Conference on Computer Vision and Pattern Recognition (CVPR) 2016:2782–2790
86. Guo X, Li Y, Ling H (2017) Lime: low-light image enhancement via illumination map estimation. IEEE Trans Image Process 26(2):982–993
87. Li M, Liu J, Yang W, Sun X, Guo Z (2018) Structure-revealing low-light image enhancement via robust retinex model. IEEE Trans on Image Process 27(6):2828–2841
88. Ren X, Yang W, Cheng W, Liu J (2020) Lr3m: robust low-light enhancement via low-rank regularized retinex model. IEEE Trans on Image Process 29:5862–5876
89. Xu J, Hou Y, Ren D, Liu L, Zhu F, Yu M, Wang H, Shao L (2020) Star: a structure and texture aware retinex model. IEEE Trans on Image Process 29:5022–5037
90. Tang M, Xie F, Zhang R, Jiang Z, Bovik AC (2020) A local flatness based variational approach to retinex. IEEE Trans on Image Process 29:7217–7232
91. Eckhorn R, Reitboeck H, Arndt M, Dicke P (2014) Feature linking via synchronization among distributed assemblies: simulations of results from cat visual cortex. Neural Comput 2(3):293–307
92. Reitboeck HJ (1989) A model for feature linking via correlated neural activity, Synergetics on Cognition
93. Parodi O, Combe P, Ducom JC (1996) Temporal coding in vision: coding by the spike arrival times leads to oscillations in the case of moving targets. Biol Cybern 74(6):497–509
94. Rybak IA, Shevtsova NA, Podladchikova LN, Golovan AV (1991) A visual cortex domain model and its use for visual information processing. Neural Netw 4(1):3–13
95. Chen Y, Park S-K, Ma Y, Ala R (2011) A new automatic parameter setting method of a simplified pcnn for image segmentation. IEEE Trans on Neural Netw 22(6):880–892
96. Ranganath H, Kuntimad G, Johnson J (1995) Pulse coupled neural networks for image processing. Proc IEEE Southeastcon'95. Visualize the Future, IEEE, pp 37–43

97. Lindblad T, Kinser JM, Taylor J (2005) Image processing using pulse-coupled neural networks. Springer, Berlin
98. Junying Z, Tao L (2003) Enhancement of image by pcnn. Comput Eng Appl 39(19):93–95
99. Kinser JM, Lindblad T (1999) Implementation of pulse-coupled neural networks in a cnaps environment. IEEE Trans Neural Netw 10(3):584–590
100. Lindblad T, Kinser JM (1999) Inherent features of wavelets and pulse coupled networks. IEEE Trans Neural Netw 10(3):607–614
101. Kuntimad G, Ranganath HS (1999) Perfect image segmentation using pulse coupled neural networks. IEEE Trans Neural Netw 10(3):591–8
102. Ranganath HS, Kuntimad G (1996) Iterative segmentation using pulse-coupled neural networks, In: Applications and Science of Artificial Neural Networks II, Vol. 2760, International Society for Optics and Photonics, pp. 543–554
103. Sun Z, Diao M, Zhao Z (2006) Algorithm of texture image enhancement based on pcnn. Appl Sci Technol 10:5–8
104. Dengchao F, Zhaoxuan Y, Zengmin W (2007) Adaptive enhancement algorithm of color image based on improved pcnn, In: 2007 8th International Conference on Electronic Measurement and Instruments, IEEE, 2007, pp. 844–848
105. Yang X, Liu T, Li X (2016) Study on image enhancement algorithm merged wavelet transform and improved pcnn [j]. Comput Eng Appl 52(8):163–168
106. Lei L, Xi F, Chen S (2019) Finger-vein image enhancement based on pulse coupled neural network. IEEE Access 7:57226–57237
107. Li G-Y, Li H-G, Wu T-H, Dong M (2005) Applications of pcnn and otsu theories for image enhancement. J Optoelectron Laser 16(3):358–362
108. Li G, Li H, Wu T (2005) The image enhancement based on modified pulse coupled neural network and genetic algorithm. J Test Meas Technol 19(3):304–309
109. Li G-Y, Li H-G, Wu T-H (2005) Enhancement of image based on otsu and modified pcnn [j]. Acta Simulata Systematica Sinica 6:1370–1372
110. Qi C-L, Ma Y-D, Zhang Z-F (2006) Study on feedback pulse-coupled neural network model and its application. Radio Eng China 36(11):59–62
111. Nie R, He M, Cao J, Zhou D, Liang Z (2019) Pulse coupled neural network based mri image enhancement using classical visual receptive field for smarter mobile healthcare. J Ambient Intell Hum Comput 10(10):4059–4070
112. Johnson JL, Padgett ML (1999) Pcnn models and applications. IEEE Trans Neural Netw 10(3):480–498
113. Zhan K, Zhang H, Ma Y (2009) New spiking cortical model for invariant texture retrieval and image processing. IEEE Trans Neural Netw 20(12):1980–1986
114. Zhan K, Shi J, Wang H, Xie Y, Li Q (2017) Computational mechanisms of pulse-coupled neural networks: a comprehensive review. Arch Comput Methods Eng 24(3):573–588
115. Zhan K, Teng J, Shi J, Li Q, Wang M (2016) Feature-linking model for image enhancement. Neural Comput 28(6):1072–1100
116. Zhan K, Shi J, Teng J, Li Q, Wang M, Lu F (2017) Linking synaptic computation for image enhancement. Neurocomputing 238:1–12
117. Rybak IA, Shevtsova NA, Sandler VM (1992) The model of a neural network visual preprocessor. Neurocomputing 4(1–2):93–102
118. Yang J, Wang G, Zhang Z, Lin S, Lu T, Jiang L (1996) The edge-detecting system of image based on the artificial receptive field implemented by the bacteriorhodopsin films. Acta Biophysica Sinica 04:65
119. Qi Y, Yang Z, Lian J, Guo Y, Sun W, Liu J, Wang R, Ma Y (2021) A new heterogeneous neural network model and its application in image enhancement. Neurocomputing 440:336–350
120. Huang Y, Ma Y, Li S (2015) A new method for image quantization based on adaptive region related heterogeneous pcnn, In: International Symposium on Neural Networks
121. Huang Y, Ma Y, Li S, Zhan K (2016) Application of heterogeneous pulse coupled neural network in image quantization. J Electron Imaging 25(6):061603
122. LeCun Y, Bengio Y, Hinton G (2015) Deep learning. Nature 521(7553):436–444
123. Schmidhuber J (2015) Deep learning in neural networks: an overview. Neural Netw 61:85–117
124. Shen D, Wu G, Suk H-I (2017) Deep learning in medical image analysis. Ann Rev Biomed Eng 19:221–248
125. Ignatov A, Kobyshev N, Timofte R, Vanhoey K, Van Gool L (2018) Wespe: weakly supervised photo enhancer for digital cameras, In: Proceedings of the IEEE Conference on Computer Vision and Pattern Recognition Workshops, pp. 691–700
126. Aly HA, Dubois E (2005) Image up-sampling using total-variation regularization with a new observation model. IEEE Trans Image Process 14(10):1647–1659
127. Chen Y-S, Wang Y-C, Kao M-H, Chuang Y-Y (2018) Deep photo enhancer: Unpaired learning for image enhancement from photographs with gans, In: Proceedings of the IEEE Conference on Computer Vision and Pattern Recognition, pp. 6306–6314
128. Jiang Y, Gong X, Liu D, Cheng Y, Fang C, Shen X, Yang J, Zhou P, Wang Z (2019)Enlightengan: Deep light enhancement without paired supervision, arXiv preprint arXiv:1906.06972
129. Xiong W, Liu D, Shen X, Fang C, Luo J (2020) Unsupervised real-world low-light image enhancement with decoupled networks, arXiv preprint arXiv:2005.02818
130. Yang W, Wang S, Fang Y, Wang Y, Liu J (2020) From fidelity to perceptual quality: A semi-supervised approach for low-light image enhancement, In: Proceedings of the IEEE/CVF Conference on Computer Vision and Pattern Recognition, pp. 3063–3072
131. Shin Y-G, Park S, Yeo Y-J, Yoo M-J, Ko S-J (2019) Unsupervised deep contrast enhancement with power constraint for oled displays. IEEE Trans Image Process 29:2834–2844
132. Chen Q, Xu J, Koltun V (2017) Fast image processing with fully-convolutional networks, In. IEEE International Conference on Computer Vision (ICCV) 2017:2516–2525
133. Chen C, Chen Q, Xu J, Koltun V (2018) Learning to see in the dark, In. IEEE/CVF Conference on Computer Vision and Pattern Recognition 2018:3291–3300
134. Hu Y, He H, Xu C, Wang B, Lin S (2018) Exposure: a white-box photo post-processing framework. ACM Trans Graph (TOG) 37(2):1–17
135. Yu R, Liu W, Zhang Y, Qu Z,Zhao D,Zhang B (2018) Deepexposure: Learning to expose photos with asynchronously reinforced adversarial learning, In: Advances in Neural Information Processing Systems 31, Curran Associates, Inc., pp. 2149–2159
136. Park J, Lee J, Yoo D, Kweon IS (2018) Distort-and-recover: Color enhancement using deep reinforcement learning, In: IEEE/CVF Conference on Computer Vision and Pattern Recognition 2018:5928–5936
137. Huang J, Zhu P, Geng M, Ran J, Zhou X, Xing C, Wan P, Ji X (2018) Range scaling global u-net for perceptual image enhancement on mobile devices, In: Proceedings of the European Conference on Computer Vision (ECCV) Workshops
138. Gharbi M, Chen J, Barron JT, Hasinoff SW, Durand F (2017) Deep bilateral learning for real-time image enhancement. ACM Trans Graph (TOG) 36(4):1–12
139. Lv F, Lu F, Wu J, Lim C (2018) Mbllen: Low-light image/video enhancement using cnns., In: BMVC, p. 220

140. Cai J, Gu S, Zhang L (2018) Learning a deep single image contrast enhancer from multi-exposure images. IEEE Trans Image Process 27(4):2049–2062
141. Lv F, Li Y, Lu F (2019) Attention guided low-light image enhancement with a large scale low-light simulation dataset, arXiv: 1908.00682
142. Zamir SW, Arora A, Khan S,Hayat M, Khan FS, Yang M-H, Shao L (2020) Learning enriched features for real image restoration and enhancement, arXiv preprint arXiv:2003.06792
143. Zhu M, Pan P, Chen W, Yang Y (2020) Eemefn: Low-light image enhancement via edge-enhanced multi-exposure fusion network. In: Proceedings of the AAAI Conference on Artificial Intelligence 34(7):13106–13113
144. Zhang Y, Zhang J, Guo X (2019) Kindling the darkness: A practical low-light image enhancer, In: Proceedings of the 27th ACM International Conference on Multimedia, pp. 1632–1640
145. Shen L, Yue Z, Feng F, Chen Q, Liu S, Ma J (2017) Msr-net: Low-light image enhancement using deep convolutional network, arXiv preprint arXiv:1711.02488
146. Wei C, Wang W, Yang W, Liu J (2018) Deep retinex decomposition for low-light enhancement, arXiv preprint arXiv:1808.04560
147. Shi Y, Xiaopo W, Zhu M (2019)Low-light image enhancement algorithm based on retinex and generative adversarial network, arXiv preprint arXiv:1906.06027
148. Wang Y, Cao Y, Zha Z-J, Zhang J, Xiong Z, Zhang W, Wu F (2019) Progressive retinex: Mutually reinforced illumination-noise perception network for low-light image enhancement, In: Proceedings of the 27th ACM International Conference on Multimedia, ACM, 2019, pp. 2015–2023
149. Liang J, Xu Y, Quan Y, Wang J, Ling H, Ji H (2020) Deep bilateral retinex for low-light image enhancement, arXiv preprint arXiv:2007.02018
150. Eilertsen G, Kronander J, Denes G, Mantiuk RK, Unger J (2017) HDR image reconstruction from a single exposure using deep CNNs. Acm Trans Graph 36(6):1–15
151. Yang X, Xu K, Song Y, Zhang Q, Wei X, Lau RWH (2018) Image correction via deep reciprocating hdr transformation, In: IEEE/CVF Conference on Computer Vision and Pattern Recognition 2018:1798–1807
152. Celik T, Tjahjadi T (2011) Contextual and variational contrast enhancement. IEEE Trans Image Process 20(12):3431–3441
153. Chen SD, Ramli AR (2004) Minimum mean brightness error bi-histogram equalization in contrast enhancement. IEEE Trans Consum Electron 49(4):1310–1319
154. Wang Zhou, Bovik AC, Sheikh HR, Simoncelli EP (2004) Image quality assessment: from error visibility to structural similarity. IEEE Trans Image Process 13(4):600–612
155. Shannon CE (2001) A mathematical theory of communication. Bell Syst Tech J 5(3):3–55
156. Agaian SS, Silver B, Panetta KA (2007) Transform coefficient histogram-based image enhancement algorithms using contrast entropy. IEEE Trans Image Process 16:741–758
157. Wang S, Zheng J, Hu HM, Li B (2013) Naturalness preserved enhancement algorithm for non-uniform illumination images. IEEE Trans Image Process A Publ IEEE Signal Process Soc 22(9):3538–3548
158. Kellman P, McVeigh ER (2005) Image reconstruction in snr units: a general method for snr measurement. Magn Reson Med 54(6):1439–1447
159. Chen ZY, Abidi BR, Page DL, Abidi MA (2006) Gray-level grouping (glg): an automatic method for optimized image contrast enhancement–part i: the basic method., IEEE Transactions on Image Processing A Publication of the IEEE Signal Processing Society 15 (8) 2290–302
160. Sheikh HR, Bovik AC (2006) Image information and visual quality. IEEE Trans Image Process 15(2):430–444
161. Yeganeh H, Wang Z (2013) Objective quality assessment of tone-mapped images. IEEE Trans Image Process A Publ IEEE Signal Process Soc 22(2):657–667
162. Zhang R, Isola P, Efros AA, Shechtman E,Wang O (2018) The unreasonable effectiveness of deep features as a perceptual metric, In: IEEE/CVF Conference on Computer Vision & Pattern Recognition
163. Fu X, Zeng D, Huang Y, Liao Y, Ding X, Paisley J (2016) A fusion-based enhancing method for weakly illuminated images. Signal Process 129:82–96
164. Ying Z, Li G, Gao W (2017) A bio-inspired multi-exposure fusion framework for low-light image enhancement, CoRR abs/1711.00591 arXiv:1711.00591
165. Dong X, Pang YA, Wang G,Li W, Gao Y,Yang S, et al., A fast effecient algorithm for enhancement of low lighting video, J Inf Comput Sci 7 (10) 2021–2030
166. Nakai K, Hoshi Y, Taguchi A, (2013) Color image contrast enhacement method based on differential intensity, saturation gray-levels histograms, In: International symposium on intelligent signal processing and communication systems. IEEE 2013:445–449
167. Ren X, Li M, Cheng W-H, Liu J, Joint enhancement and denoising method via sequential decomposition, In: (2018) IEEE International Symposium on Circuits and Systems (ISCAS). IEEE 2018:1–5
168. Ying Z, Li G, Ren Y, Wang R, Wang W (2017) A new low-light image enhancement algorithm using camera response model. In: Proceedings of the IEEE International Conference on Computer Vision Workshops 2017:3015–3022
169. Wang R, Zhang Q, Fu C-W, Shen X, Zheng W-S, Jia J (2019) Underexposed photo enhancement using deep illumination estimation, In: Proceedings of the IEEE Conference on Computer Vision and Pattern Recognition, pp. 6849–6857
170. Wang W, Wei C, Yang W, Liu J, Gladnet: Low-light enhancement network with global awareness, In: 2018 13th IEEE International Conference on Automatic Face & Gesture Recognition (FG 2018), IEEE, 2018, pp. 751–755
171. Lore KG, Akintayo A, Sarkar S (2017) Llnet: a deep autoencoder approach to natural low-light image enhancement. Pattern Recognit 61:650–662